Cell. Mol. Life Sci. 64 (2007) 1085 – 1104
1420-682X/07/091085-20
DOI 10.1007/s00018-007-6447-x

Cellular and Molecular Life Sciences

Review

Investigating metal-binding in proteins by nuclear magnetic resonance

M. Ringkjøbing Jensen, M. A. S. Hass, D. F. Hansen[+] and J. J. Led[*]

Department of Chemistry, University of Copenhagen, Universitetsparken 5, 2100 Copenhagen Ø (Denmark)
Fax: +45 35 32 03 22, e-mail: led@kiku.dk

Received 12 October 2006; received after revision 30 November 2006; accepted 5 February 2007
Online First 31 March 2007

Abstract. Metal ions play a key role for the function of many proteins. The interaction of the metal ion with the protein and its involvement in the function of the protein vary widely. In some proteins, the metal ion is bound tightly to the ligand residues and may be the key player in the function of the protein, as in the case of blue copper proteins. In other proteins, the metal ion is bound only temporarily and loosely to the protein, as in the case of some metalloenzymes and other proteins where the metal ion acts as a cofactor necessary for the function of the protein. Such proteins are often known as metal ion-activated proteins. The review focuses on recent nuclear magnetic resonance (NMR) studies of a series of metal-dependent proteins and the characterization of the metal-binding sites. In particular, we focus on NMR techniques for studying metal binding to proteins such as chemical shift mapping, paramagnetic NMR and changes in backbone dynamics upon metal binding.

Keywords. NMR, chemical shift mapping, backbone dynamics, paramagnetic NMR, calmodulin, zinc finger, plastocyanin, prion protein.

Introduction

Metal ions are essential for the biological function of many proteins. Thus, at least one-third of all proteins encoded in the human genome appear to contain metal ions which perform a wide range of specific functions [1]. Traditionally, metalloproteins have been viewed as robust metal complexes with high-affinity metal-binding sites, which bind metal ions tightly in a well-defined coordination. Examples of robust metalloproteins are the blue copper proteins, such as plastocyanin [2], where the metal ion is essential for the redox activity of the protein but has little impact on its overall structure. Yet, the geometric and the electronic structure of the metal-binding site are essential for the function [3–5]. Another class of metalloproteins with tightly bound metal ions are the zinc finger proteins, where the metal ion keeps the protein in the correct folding or structure necessary for its activity, but has little functional importance itself [6, 7]. Other proteins where metal ions are of structural importance are many regulatory proteins, where the function relies on a metal ion-induced switch between different forms of the protein with different biological activities. Such proteins are also known as metal ion-activated proteins [8], the calcium-binding proteins of the calmodulin family being one of the most studied examples [9]. In these proteins, the metal binding *in vivo* is temporary and

[+] Present address: Department of Medical Genetics and Microbiology, University of Toronto, 1 King's College Circle, Toronto, ON, M5S 1A8 (Canada)
[*] Corresponding author.

the metal affinity is closely matched to the *in vivo* concentration of the relevant metal ions.

Other examples of metal ion-activated proteins are the Mg^{2+} or Zn^{2+}-dependent tRNA synthetases [10, 11] that play a key role in protein biosynthesis, and proteins involved in pathogenesis, in particular those causing neurodegenerative diseases such as Parkinson, Alzheimer, and Creutzfeldt-Jakob and other prion diseases [12]. These proteins require metal ions for at least some of their functions, although in many cases the function of the ion is unclear. Furthermore, for these proteins, the specific metal-binding sites are often poorly characterized or even unknown, and the characterization of the metal-protein interactions includes a determination of the binding constants and the metal ion exchange rates, as well as the location of the metal binding sites. Finally, also metal transporting proteins, and proteins that use metal ions for stabilization during storage, for example, insulin and human growth hormone, both of which are stabilized by Zn^{2+} [13, 14], also only bind metal ions temporarily.

This review focuses on the use of nuclear magnetic resonance (NMR) spectroscopy to study metalloproteins and metal-protein interactions. To illustrate this, we shall focus on a series of important protein studies that have recently clarified the binding and the function of the metal ion. In particular, we shall emphasize NMR techniques for locating and characterizing the metal-binding sites in proteins that bind metal ions only weakly or temporarily, and for determining the geometric and electronic structure of the metal-binding site of blue copper proteins. We will also examine the use of protein dynamics to obtain information about metal-protein interactions.

Monitoring metal ion binding in proteins by NMR

Identification of the metal-binding sites in proteins and mapping the structural and dynamic changes upon metal binding are important for our understanding of the biological function of metal-dependent proteins. Today, NMR spectroscopy is one of the leading techniques for this purpose since it provides information at the atomic level about the structure and dynamics of proteins in solution.

In practice, NMR studies of proteins are restricted to relatively small, soluble proteins ($M_w < 40$ kDa). Larger proteins often give rise to spectral overlap because of the increased number of signals and the enhanced line widths of the resonances. This is the case even for two- and three-dimensional NMR spectra. The problem can to some extent be solved by isotopic labeling of the proteins, for example with ^{15}N and/or ^{13}C isotopes. A whole range of NMR experiments (triple resonance) are available that correlate the ^{1}H, ^{15}N, and ^{13}C nuclei [15]. Furthermore, the line broadening inherently associated with large molecular-weight complexes can be reduced by per-deuterating the proteins and by utilizing the transverse relaxation optimized spectroscopy (TROSY) technique [16]. In recent years, strategies for isotopic enrichment of proteins have improved considerably, making labeling a standard procedure in modern NMR spectroscopy of proteins.

The protein sample must meet certain requirements that depend on the specific kind of study. For example, the solution structure of small globular proteins ($M_w <$ 15 kDa) can often be determined without any isotopic labeling. On the other hand, NMR studies of the backbone dynamics of a protein require that it is ^{15}N labeled. For large proteins, isotope labeling with both ^{15}N and ^{13}C is required to obtain the assignment of the protein resonances, which, in turn, is a necessary prerequisite for studying the structure and dynamics of the protein.

The protein concentrations typically used in NMR studies are in the range from 0.1 to 2.0 mM. The higher concentrations may be an advantage, since they reduce the amount of time necessary to record high-resolution spectra. However, they may also result in a weak aggregation of the protein that causes a broadening of the NMR signals, hence reducing the spectral resolution. The signal-to-noise ratio and the spectral dispersion both increase as the magnetic field strength is increased. Thus, in general, the quality of the NMR spectra depends on both the protein concentration and the magnetic field strength. Today state-of-the-art NMR spectrometers operate at ^{1}H frequencies up to 900 MHz. Yet, a ^{1}H frequency of 500 MHz may suffice in many cases, in particular if the spectrometer is equipped with a high-sensitive cryogenic probe. Below, we describe a series of NMR approaches that are useful for monitoring metal ion binding to proteins. Since the binding of diamagnetic and paramagnetic metal ions affects the protein NMR spectra in rather different ways, the two cases are discussed separately.

Diamagnetic metal ions

The binding of diamagnetic metal ions to proteins can be studied conveniently through the chemical shift perturbations caused by the metal ion binding. This approach is usually denoted as 'chemical shift mapping' [17–19]. The chemical shift perturbations can be followed in titration experiments, where the concentration of the diamagnetic metal ion is increased

gradually. The chemical shift perturbations stem mainly from structural changes caused by the metal binding, and from the electric field induced by the charge of the metal ion. Chemical shift mapping provides information about the location of the metal-binding site(s).

If the exchange between the metal-free and the metal-bound form of the protein is slow compared to the chemical shift difference between the two forms ($k_{ex} \ll \Delta\omega$), separate NMR signals are observed for the two forms of the protein. Here, k_{ex} is the rate of exchange between the two forms and is given by

$$k_{ex} = k_{on}[\mathrm{Me}] + k_{off} = \frac{k_{off}}{1-f} \quad (1)$$

where [Me] is the metal ion concentration, f is the fraction of the metal-bound protein, k_{on} is the second-order rate constant for the complex formation, and k_{off} is the first-order rate constant for the complex dissociation. While the chemical shifts of the two signals will remain unchanged as a function of the metal ion concentration, the signal intensities will change with the metal ion concentration, allowing determination of the fraction of the metal-bound protein. On the other hand, if the exchange between the metal-free and the metal-bound form of the protein is fast compared to the chemical shift difference between the two forms ($k_{ex} \gg \Delta\omega$), a single exchange-averaged signal is observed. The chemical shift of the exchange-averaged signal will depend on the metal ion concentration. Thus, the protein-metal binding constant can be estimated from the variation in the chemical shifts with the metal ion concentration.

Chemical shift mapping with diamagnetic metal ions does not, in general, provide information about the geometric structure of the metal-binding sites since most often these ions are NMR silent and, therefore, do not interact magnetically with the nuclei of the ligand residues. Nevertheless, the position of these residues, and the structure of the protein framework adjacent to the metal ion, can be obtained from the short-range inter-proton distances (<5Å) derived from the nuclear Overhauser enhancements (NOEs) [20, 21]. Even more detailed information can be obtained if the metal ion is substituted for an NMR-active metal. Thus, $^{111/113}$Cd, ^{199}Hg and ^{109}Ag have proved useful in studies of biological systems [22]. For example, the ^{113}Cd chemical shift is very sensitive to the nature, number and geometric arrangement of the coordinating ligands. Furthermore, the coupling constants between the NMR active metals and nuclei of the protein provide insight into the identity and geometry of the metal ligands [22]. Finally, it should be noted that the overall geometric structure of the binding site, including the location of the metal ion, can be determined by X-ray crystallography, provided that well-defined crystals of the protein can be obtained.

In addition to the structural changes mentioned above, the flexibility of the protein may also change upon metal ion binding. In particular, a decrease in the flexibility of the protein close to the metal-binding site may be observed. These changes in dynamics not only indicate the location of the metal-binding site, they may also be important for the biological function of the proteins [23]. NMR spectroscopy can provide detailed information at the atomic level about the backbone dynamics on the pico- to hanosecond time scale and exchange processes on the micro- to millisecond time scale in proteins [24–26], a time scale characteristic for many enzymatic processes. In contrast to conventional methods for studying kinetics, conformational changes at equilibrium conditions can be studied by NMR [26]. Therefore, no chemical perturbation of the system of interest is required.

Dynamics information can be retrieved from the ^{15}N R_1 and R_2 relaxation rates and the $\{^1\mathrm{H}\}$–^{15}N NOE of the backbone ^{15}N nuclei of the protein [27]. Information on the side chain dynamics can be obtained using the relaxation rates of the ^{13}C, ^{1}H or ^{2}H nuclei of methyl groups [28, 29]. In general, the longitudinal relaxation rate, R_1, and the heteronuclear NOE are sensitive only to molecular motions taking place on the pico- to nanosecond time scale, whereas the R_2 relaxation rate depends on motions taking place on both that and the micro- to millisecond time scale. In many studies, the NOE is used as a qualitative measure of internal dynamics on the pico- to nanosecond time scale.

The dynamics information is obtained from the relaxation parameters using the so-called model-free formalism [30, 31], where "model-free" indicates that no specific assumptions are made regarding the exact motions of the atoms. A detailed description of the model-free formalism and the procedure for analyzing the experimental relaxation parameters can be found elsewhere [27]. In the case of highly flexible molecules, such as unfolded proteins, the model-free formalism is not applicable. For such systems the relaxation parameters are usually interpreted using spectral density mapping [26].

A model-free analysis of the relaxation data provides an order parameter, S^2, and an exchange term, R_{ex}, for each residue, and the overall correlation time, τ_r, for the rotational reorientation of the protein. The S^2 parameters describe motions in the protein on the pico- to nanosecond time scale. More specifically, S^2 provides information about the fluctuation of the amide ^{15}N-^{1}H bond of a given residue. Thus, $S^2 = 0$

corresponds to a completely flexible ^{15}N-^{1}H bond vector, while $S^2=1$ corresponds to a ^{15}N-^{1}H bond vector with no motion. The R_{ex} term gives information about exchange processes on the micro- to millisecond time scale taking place in the protein. It depends on the exchange rate, the populations of the exchanging conformations, their chemical shift difference, the magnetic field strength, and on the rate of a series of pulses (the pulse rate of the so-called CPMG experiment [24, 32, 33]), or the strength of the spin-lock field, depending on the specific NMR experiment being used to measure the R_2 rate [34]. Often, the R_{ex} terms can only be interpreted qualitatively. The R_{ex} terms give qualitative information about the location of conformational exchange processes in the protein [35]. Residues with exchange terms may cluster in specific regions of the protein, suggesting that these residues are affected by one and the same conformational exchange process. Furthermore, the temperature dependence of R_{ex} provides information about the time-scale of the exchange process [36]. In special cases, exchange contributions can be interpreted quantitatively, if additional information is available about exchange rates, thermodynamic parameters or chemical shift amplitudes [26, 35]. This information can in some cases be obtained from CPMG relaxation dispersion experiments and $R_{1\rho}$ dispersion experiments [34].

Paramagnetic metal ions

The binding of paramagnetic metal ions to proteins has a much more dramatic effect on the NMR spectra of the protein than the binding of diamagnetic metal ions. Therefore, monitoring the binding of a paramagnetic metal ion to a protein by NMR is very different from the diamagnetic case. The reason for the dramatic effect is the strong interactions between the unpaired electrons of the metal ion and the surrounding protein nuclei. Thus, the presence of unpaired electrons affects both the chemical shifts and the relaxation rates of the protein nuclei.

The chemical shift of a nucleus in a paramagnetic metal complex is given by the sum of two contributions, a diamagnetic contribution which is the observed chemical shift in an analogue diamagnetic compound, and a paramagnetic contribution, consisting of the contact shift and the pseudocontact shift [37]. The contact shift is a through-bond effect caused by the scalar coupling between the nuclei and the unpaired electron(s) of the metal ion. It affects nuclei only a few bonds away from the metal ion. Scalar coupling is often responsible for shifting signals of nuclei in the immediate vicinity of the metal site to extreme chemical shifts. The pseudocontact shift is a through-space effect caused by an interaction between the magnetic dipoles of the nuclei and the unpaired electron(s). It affects the nuclei within a large range of distances from the metal ion, that is, up to 35 Å from the metal ion, depending on the anisotropy of the g-tensor and the electron spin quantum number. In particular, the pseudocontact shifts of the protein nuclei are valuable because they depend on the spherical position of the nuclei with respect to the metal ion. Therefore, the pseudocontact shifts have been used extensively to refine the solution structures of native metalloproteins. Recent reviews have been written on the use of paramagnetic restraints in the structure determination of native metalloproteins [38, 39]. Paramagnetic restraints have also been used in the structure determination of non-metalloproteins. In these studies, the paramagnetic metal ion was incorporated into the proteins using metal-binding tags [40–50].

The relaxation rates of the nuclei in a paramagnetic protein contain information about the location of the metal ion and the geometry of the metal site, as well as information about the electronic structure of the site. This multitude of information is a result of the interaction between the magnetic dipoles of the nuclei and the unpaired electron(s). Thus, in a paramagnetic protein the observed nuclear relaxation rate, R_{io}, is given by

$$R_{io} = R_{id} + R_{ip} \quad i = 1, 2 \tag{2}$$

Here, $i=1$ is the longitudinal relaxation rate and $i=2$ is the transverse relaxation rate, where the latter is given by the linewidth of the signal. Furthermore, R_{id} is the relaxation rate observed in an analogue diamagnetic compound, and R_{ip} is the paramagnetic relaxation enhancement caused by the interaction between the nucleus and the unpaired electrons of the paramagnetic metal ion. In cases where the interaction is purely dipolar, the longitudinal, R_{1p}, and the transverse, R_{2p}, paramagnetic relaxation enhancements are given by [51]

$$R_{1p} = \frac{2}{15}\left(\frac{\mu_0}{4\pi}\right)^2 S(S+1) g_e^2 \mu_B^2 \gamma_I^2 r^{-6} \times \left[\frac{3\tau_{c,1}}{1+\omega_I^2\tau_{c,1}^2} + \frac{7\tau_{c,2}}{1+\omega_S^2\tau_{c,2}^2}\right] \tag{3}$$

$$R_{2p} = \frac{1}{15}\left(\frac{\mu_0}{4\pi}\right)^2 S(S+1) g_e^2 \mu_B^2 \gamma_I^2 r^{-6} \times \left[4\tau_{c,1} + \frac{3\tau_{c,1}}{1+\omega_I^2\tau_{c,1}^2} + \frac{13\tau_{c,2}}{1+\omega_S^2\tau_{c,2}^2}\right] \tag{4}$$

where, μ_0 is the permeability of free space, S is the electron spin quantum number, and g_e is the electron g-factor. μ_B is the Bohr magneton, γ_I is the gyromag-

netic ratio of the nuclear spin, I, and r is the distance between the unpaired electrons and the nucleus. Finally, ω_I and ω_S are the Larmor frequencies of the nuclear spin, I, and the electron spin, S, respectively. The correlation times, $\tau_{c,1}$ and $\tau_{c,2}$ are given by [52]

$$\tau_{c,1} = (\tau_r^{-1} + R_{1e})^{-1} \quad (5)$$

$$\tau_{c,2} = (\tau_r^{-1} + R_{2e})^{-1} \quad (6)$$

where R_{1e} and R_{2e} are the longitudinal and the transverse electron relaxation rates, respectively, and τ_r is the correlation time for the rotational reorientation of the complex. Both the electron relaxation rates [53] and the rotational correlation time of the protein [24] can be determined by NMR relaxation measurements.

From equations 3 and 4, it can be seen that the paramagnetic relaxation enhancements contain information about the distance, r, between the metal ion and the protein nuclei. Thus, by measuring the paramagnetic relaxation enhancements for a sufficient number of protein nuclei, the location of the paramagnetic metal ion can be determined. This has been demonstrated for the calcium-binding protein calbindin D_{9k}, where the calcium ion was substituted by the paramagnetic lanthanide ion, Ce^{3+} [54], and the location of the metal ion in the protein structure was determined from the interactions between the unpaired electrons and the protein nuclei.

The R_{2p} relaxation and, thus, the line broadening observed in paramagnetic metalloproteins can be very severe. The signals of nuclei close to the metal ion may be broadened beyond detection, so that information about the geometric structure of the protein close to the metal site cannot be obtained. An example of that is the 109-amino acid protein oncomodulin that contains two Ca^{2+}-binding sites. Upon substitution of one of the calcium ions with Tb^{3+}, ^1H-^{15}N heteronuclear single-quantum coherence (HSQC) cross-peaks are detectable only beyond 16 Å from the paramagnetic metal [55]. However, it has been recently shown that a significant improvement in the 'visibility' close to the metal ion can be achieved by direct ^{13}C detection [55–57]. Due to the lower gyromagnetic ratio of ^{13}C nuclei compared to protons, the line broadening effects are less severe for ^{13}C nuclei. Thus, in the Tb^{3+}-substituted oncomodulin, signals of ^{13}C nuclei as close as 8 Å to the metal site were observed detected using two-dimensional directly detected ^{13}C experiments [55]. Direct detection of ^{13}C may also be an advantage in cases where signals are lost in the ^1H-^{15}N HSQC spectrum due to fast amide proton exchange [57]. It should also be noted that electron paramagnetic resonance (EPR) and electron-nuclear double resonance (ENDOR) experiments can provide detailed structural information about the metal-binding sites in native metalloproteins [58, 59].

Proteins with less specific metal ion binding, examples of which are described in this review (see below), may have a number of different binding sites on the protein surface, each of which may have different occupancies. In such cases, characterization of the metal-protein interaction is less straightforward. Using X-ray crystallography, determination of the location of the binding sites can be difficult if the occupancies of the binding sites are low. However, if the metal ion is paramagnetic, even low-populated binding sites can be detected by NMR. Thus, upon binding of a paramagnetic metal ion to a protein, the relaxation rates of the protein nuclei are enhanced due to the interactions with the unpaired electrons of the paramagnetic ion. The relaxation enhancements depend on the distance, r, between the paramagnetic metal ion and the protein nuclei, the effect diminishing according to the inverse-sixth power of the interatomic distance (see Eqs. 3 and 4). Consequently, selective broadening of the NMR signals of the nuclei spatially close to the metal-binding site is observed, indicating the location of the binding site. For proteins, where only a fraction of the molecules are metal bound, the NMR line broadening upon metal binding depends on the metal-bound fraction, which must therefore also be determined if a more quantitative characterization of the binding site is to be obtained [60–62]. Furthermore, different paramagnetic metal ions have different line-broadening effects, since the line-broadening effects are controlled primarily by the electron spin quantum number and the size of the relaxation rates of the unpaired electrons of the paramagnetic metal ion (see Eqs. 3–6). Thus, Cu^{2+}, which has a relatively slow electron relaxation rate, induces severe line-broadening effects, while the paramagnetic Ni^{2+} ion, for example, which has a relatively fast electron relaxation rate, only induces a modest line broadening. An overview of the line broadening induced by different paramagnetic metal ions can be found in Bertini et al. [63]. Finally, it should be noted that studies of the backbone dynamics of paramagnetic metalloproteins using NMR relaxation and the model-free approach [30, 31] are difficult since the paramagnetic relaxation enhancements obscure the ^{15}N relaxation rates. Therefore, only a few studies of the backbone dynamics of paramagnetic proteins have been reported [64, 65].

Applications

We will now focus on a series of recent NMR studies of metal-dependent proteins. These include investigations of calmodulin, zinc fingers, plastocyanin, α-synuclein and prion proteins. In particular, we focus on the use of NMR to characterize the metal-binding sites in these proteins and to provide insight into the dynamic events that take place upon metal binding, through measurements of protein backbone dynamics.

EF-hands

EF-hands are common calcium-binding motifs in eukaryotes, present in proteins such as aequorin, calbindin D9k, troponin C, recoverin and calmodulin. The calcium-binding EF-hand motif consists of two α-helices connected by a calcium-binding loop, although magnesium binds as well.

An example of how NMR chemical shift mapping can be used to clarify details about the biological function of an EF-hand is aequorin. Aequorin is a light-emitting protein isolated from jellyfish. Calcium binding triggers the emission of blue light from a coelenterazine cofactor in complex with aequorin. It has frequently been utilized as an intracellular calcium sensor. Aequorin consists of four EF-hands, I–IV, forming a compact globular structure [66]. Three of the EF-hands can bind a calcium ion, however only two calcium ions are required for luminescence. Aequorin can also bind magnesium ions, which inhibit luminescence, also at *in vivo* concentrations. Chemical shift mapping has been used to investigate Mg^{2+} binding to aequorin [67]. Large differences in the chemical shift between Mg^{2+}-bound and apo-aequorin are observed in the I and III EF-hands, whereas the loops II and IV only show minor changes (see Fig. 1). Thus, only two of the EF-hands in aequorin have a significant affinity for Mg^{2+}.

As aequorin, many proteins use metal-binding sites as switches, where metal ions are used to regulate the secondary and tertiary structure. Metal ions that bind to proteins can change the overall protein structure and thereby control the biological activity of the protein. Such metal-induced allosteric switches are highly utilized in biological signal transfer. The EF-hand protein most extensively studied by NMR is calmodulin. Calmodulin is a key component of intracellular signaling pathways, such as insulin release, muscle contraction and triggering of cell death, through its activation of several kinases and phosphokinases. Over a hundred different proteins are known to bind calmodulin. This diversity of regulatory functions is thought to be accomplished by the ability of calmodulin to adopt different conformations, which is closely coupled to calcium binding [68, 69].

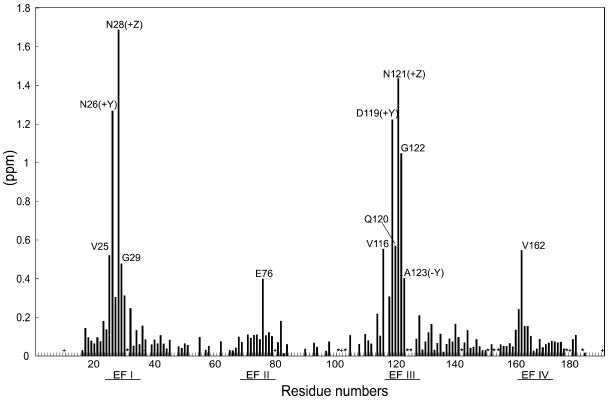

Figure 1. The absolute value differences of amide proton chemical shifts between Mg^{2+}-free and Mg^{2+}-bound aequorin. The loop regions of EF-hands I–IV are indicated by lines. Proline residues are indicated by (+) marks. The asterisks (*) represent uncalculated residues. Reproduced with permission from J. Biochem. (2005) vol. 138, pp. 613–620. Copyright 2005 Oxford University Press.

Calmodulin consists of two largely independent domains joined by a flexible α-helical tether [70], where each domain consists of two EF-hands linked together (see Fig. 2). The calcium ion is coordinated in a pentagonal bipyramidal geometry to one glutamate and three aspartate side chains, one backbone carbonyl and a water molecule [71]. X-ray [72–74] and NMR [75–77] structures of calmodulin in the presence and absence of calcium ions reveal large differences between calcium-loaded calmodulin and the apo-protein. The apo-protein forms a compact structure referred to as the 'closed' state with hydrophilic side chains on the surface and hydrophobic groups in the core. Upon calcium binding, the protein flips into an 'open' structure, where a large part of the hydrophobic core is exposed to the surface by changing the relative orientation of the four α-helices (see Fig. 2). This hydrophobic surface is the main binding interface between calmodulin and its target molecules [68, 69].

^{15}N NMR relaxation measurements have been used to analyze the dynamic transition between the 'open' and 'closed' states, which occurs on the microsecond time scale. These studies suggest that, in solution, the equilibrium between the 'open' and 'closed' state is pre-existing in the apo-form, but that it is strongly shifted towards the 'closed' form [78–80]. Binding of one calcium ion shifts the equilibrium towards the 'open' state, and when both EF-hands within the same domain bind calcium, the equilibrium is strongly shifted towards the 'open' conformation. Furthermore, the binding of two Ca^{2+} ions to one calmodulin domain is found to be strongly cooperative [81].

The exchange between the 'open' and 'closed' conformations has been studied extensively by NMR for

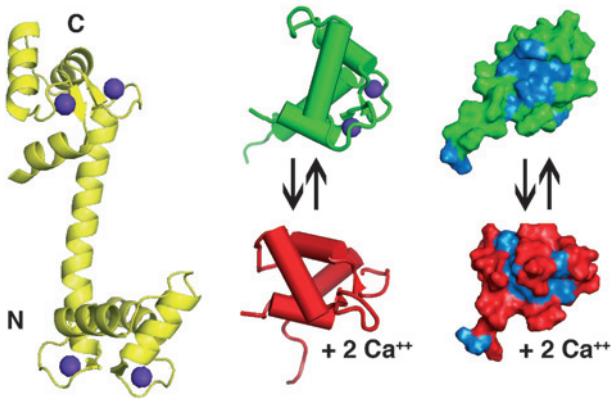

Figure 2. Structures of calmodulin. Shown in yellow is the crystal structure of Ca^{2+}-loaded calmodulin [74], demonstrating both the N-and C-terminal domain each formed of two calcium-bound EF-hands. The solution NMR structure of the C-terminal domain of calmodulin in the 'open' calcium-loaded state is shown in green, and in the 'closed' calcium-free state in red [77]. Purple: the location of the calcium ions according to the crystal structure [74]. Blue: hydrophobic residues on the surface of calmodulin showing the formation of a hydrophobic binding site upon Ca^{2+} binding. The figure was created with PyMOL [181].

wild-type (WT) and mutant calmodulins. These studies utilize the exchange contributions, R_{ex}, to the R_2 relaxation rates caused by the exchange between 'open' and 'closed' conformations or between calcium-bound and calcium-free calmodulin. The exchange contributions caused by this exchange in calcium-loaded E140Q calmodulin are shown in Figure 3. It can be seen that the exchange affects almost all backbone ^{15}N nuclei in the protein. In addition $R_{1\rho}$ relaxation dispersion experiments have proved useful for determining the exchange rate, which is about $5 \times 10^4\ s^{-1}$ [80].

Studies of two mutants of the C-terminal domain of calmodulin, namely the E104Q and E140Q mutants, have provided new insight into the calcium-binding ability of calmodulin. In each mutant, one of the calcium-binding glutamates was changed to a glutamine: in the N-terminal binding site, E104, and in the C-terminal binding site, E140. In both cases, the calcium-binding affinity was reduced dramatically in the N- and C-terminal binding site, respectively. Consequently, the cooperative calcium binding is replaced by a sequential binding mode, as shown by chemical shift titrations [82, 83]. Thus, in the E140Q mutant, the first calcium ion binds the N-terminal binding site and the second ion binds the C-terminal site. The reverse is the case for the E104Q mutant. To understand the mechanism underlying the allosteric transition of calmodulin associated with the cooperative binding of calcium ions, it is important to address the question: which site binds the first calcium ion in the WT protein? Because of the strong positive cooperativity between the sites in the WT protein, and because the single calcium-bound form is always low populated, it is not possible to answer this question directly from chemical shift titrations. The question was answered by NMR relaxation measurements of the apo-form at low calcium concentrations. Under these conditions, the apo-form is in equilibrium with a low-populated, single calcium-bound form. In addition to this equilibrium, the 'closed' conformation exchanges with the 'open' conformation of the apo-form; however, the two processes could be separated by their dependence on the calcium concentration. The exchange contribution to the R_2 relaxation rate is closely related to the difference in chemical shift between the exchanging forms of the protein. The R_{ex} contributions were found to correlate with the difference in chemical shift between the apo-form and the single calcium-bound form of the E104Q mutant, but not that of the E140Q mutant. Thus, relaxation measurements on the C-terminal domain of WT calmodulin combined with chemical-shift data from the mutant show that the first calcium ion preferentially binds the C-terminal EF-hand [78, 79] in the WT protein.

The cooperative binding of calcium in WT calmodulin may be associated with changes in the dynamics of the calcium-binding loops induced by the metal binding. Here, ^{15}N NMR relaxation studies of the backbone dynamics on the pico- to nanosecond time scale show that in the apo-protein, the calcium-binding loops are highly flexible, whereas in the calcium-bound form, the loops are rigid [70, 78, 79, 84]. This can be seen by the enhanced-order parameters in the calcium-bound form compared to the apo-form in Figure 3.

Finally, ^{43}Ca NMR line shape analysis and more conventional ^{15}N and ^{1}H NMR have been used to study the competitive binding of magnesium ions [85, 86]. These studies show that although calmodulin binds Mg^{2+} with an affinity four orders of magnitude smaller than Ca^{2+}, calmodulin still binds Mg^{2+} to a significant degree at physiological conditions, where the concentration of free Mg^{2+} ions is two to four orders of magnitude higher than the Ca^{2+} concentration. However, in contrast to calcium binding, magnesium binding seems not to induce the conformational change from the 'closed' to the 'open' state.

Zinc finger

Some metalloproteins assume their native structure even in the absence of metal ions. For example, the blue copper protein azurin folds in the absence of metal ions into a native-like structure, with a preformed metal-binding site, which can subsequently bind a copper ion [7, 87]. Thus, the metal ion is not essential for the folding. A very different scenario is

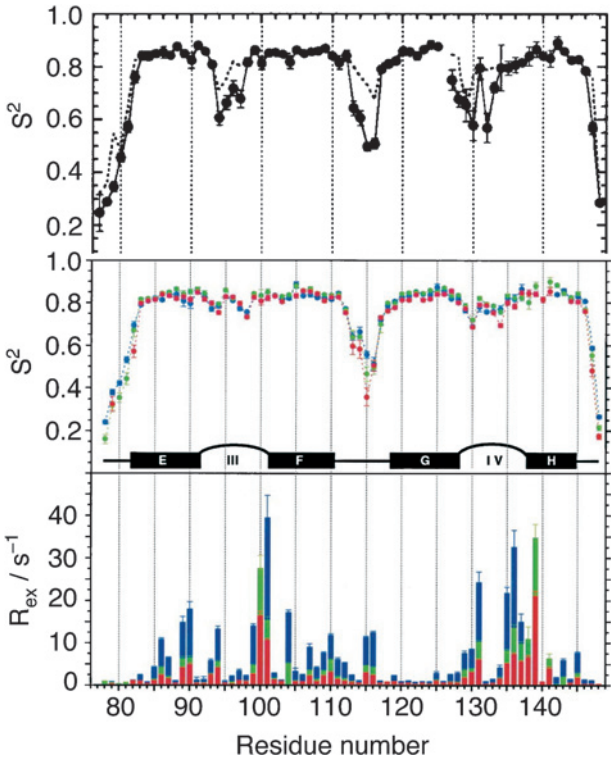

Figure 3. The backbone amide order parameters, S^2, of the C-terminal domain of apo-calmodulin (upper panel), calcium-loaded E140Q calmodulin (middle panel), and the μs-ms exchange contributions R_{ex} to the ^{15}N R_2 rates of calcium-loaded E140Q calmodulin (lower panel). All data were obtained from ^{15}N NMR relaxation measurements at 18 °C (blue), 28 °C (green) and 35 °C (red). Measurements on apo-calmodulin were done at 18 °C. The horizontal bars indicate the α-helices and the arcs indicate the calcium-binding loops III and IV. It can be seen that the order parameters of the calcium-binding loops increase upon calcium binding, corresponding to a decrease in the flexibility on the ps-ns time scale. The R_{ex} contributions arise from the exchange on the μs time scale between the 'open' and closed 'form' of calmodulin. The upper panel reproduced with permission from J. Mol. Biol. (1999) vol. 293, pp. 883–899. Copyright 1999 Elsevier. Middle and lower panels reproduced with permission from J. Mol. Biol. (1999), vol. 289, pp. 603–617. Copyright 1999 Elsevier.

presented by the zinc finger domains, where the protein obtains its functional fold only in the presence of Zn^{2+}.

Originally, zinc fingers were discovered as a peculiar nine-fold repeat of 30 amino acids in the sequence of transcription factor IIIA of *Xenopus laevis*. This transcription factor required zinc ions for DNA binding [88]. The nine repeats all contain two cysteines and two histidines at invariant positions. This suggested that these four residues were involved in the binding of zinc ions. Other divalent metal ions such as Cd^{2+}, Co^{2+}, Ni^{2+} and Fe^{2+} bind as well, however with a much lower affinity [89, 90]. Using extended X-ray absorption fine structure (EXAFS), these four residues were confirmed to be the metal-binding ligands, binding zinc in a tetrahedral conformation [91]. Since then, NMR [92] and X-ray [93] structures have provided further insight into the structure of zinc fingers (see Fig. 4).

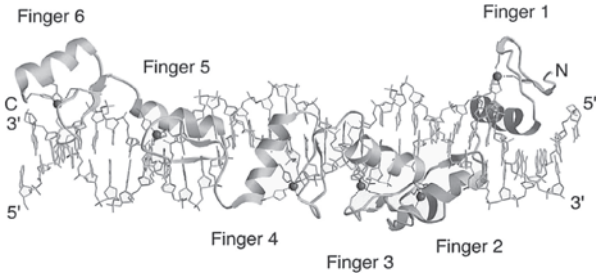

Figure 4. The structure of the six-finger TFIIIA-DNA complex. The α helices and β-sheets of TFIIIA are shown as ribbon structures. Reproduced with permission from Proc. Natl. Acad. Sci. USA (1998), vol. 95, pp. 2938–2943. Copyright 1998 Natl. Acad. Sci. USA.

Today, the zinc finger motif is known to be the most abundant DNA-binding domain present in transcription factors in eukaryotes. Furthermore, zinc finger domains are not only involved in DNA binding, but also in RNA and lipid interactions [94]. About one thousand zinc finger proteins are encoded in the human genome [95].

The classical zinc finger domain as found in transcription factor IIIA has a $\beta\beta\alpha$ fold. The zinc-binding residues are usually two cysteines and two histidines or four cysteines, however there exist a number of different variations [96]. The metal site bridges the α-helix and a β-strand, which contribute with two ligands each. The zinc ion thereby stabilizes the secondary and tertiary structure.

Removal of zinc from an isolated zinc finger causes large changes in the spectroscopic characteristics of the zinc finger peptide: the CD spectrum shows a loss in ellipticity [97], the ^{1}H NMR spectrum becomes less dispersed [6] and bands characteristic of α-helical structure become less intense in the Raman spectrum [98]. All together this shows that the metal-free peptide is relatively unstructured but folds into a more globular structure upon addition of zinc. In particular, the α-helix which contains two of the zinc ligands is unstructured in the absence of zinc. The α-helix forms the most important DNA-binding surface. However, there are zinc fingers that behave differently. Thus, the zinc finger from the human general transcription factor TFIIB is structured even in the absence of zinc. The structure of both the zinc and the apo-form were determined using NMR [99]. The two structures are very similar and the amide chemical shifts are also very similar for the two forms. However, significant differences in the $\{^1H\}$–^{15}N NOE were observed even in regions far from the metal site [99].

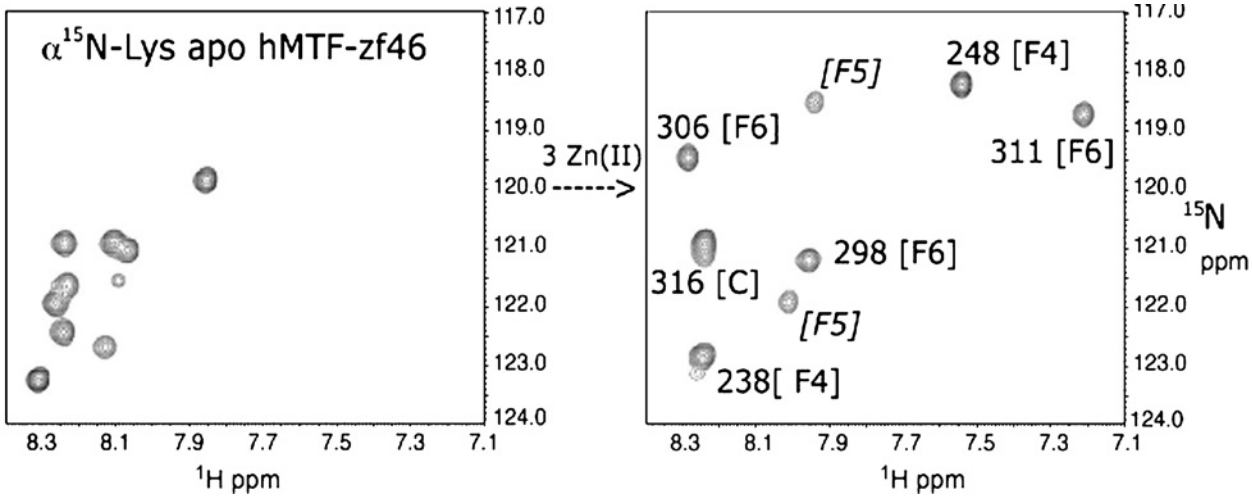

Figure 5. The ^{15}N HSQC of α ^{15}N-lysine labeled apo-form (left) and zinc-bound form (right) of the three C-terminal zinc finger domains (F4, F5 and F6) in human metalloregulatory transcription factor-1. The increase in the dispersion of the NMR signals indicates that the protein becomes more structured upon binding Zn^{2+}. Reproduced with permission from J. Biol. Chem. (2001), vol. 276, pp. 42322–42332. Copyright 2001 The American Society for Biochemistry and Molecular Biology, Inc.

This indicates that the Zn^{2+} ion stabilizes the structure and restricts the flexibility.

The more complex binding of zinc to the multiple zinc finger domain F1–F6 of the metalloregulatory transcription factor-1 (MFT-1), and the effect of zinc binding on structure and backbone dynamics, have been studied using heteronuclear ^{1}H-^{15}N NMR including NMR relaxation measurements [100, 101] (see Fig. 5). These studies show that all six zinc fingers adopt the stable $\beta\beta\alpha$ fold upon stoichiometric addition of zinc and that their binding affinities are of similar magnitude. However, studies on the F4–F6 domain suggest that even at stoichiometric zinc concentrations, the F5 zinc finger adopts different conformations and that F5 is only partially structured [100]. These findings are in contrast to a later study of the full six zinc-finger domain F1–F6 [101]. The NMR relaxation properties, the chemical shift and zinc-binding properties of F5 are similar to those of the other five zinc fingers. However, F5 has been found to be highly sensitive to thiol-oxidation. One may, therefore, speculate that oxidation of F5 is the reason for the apparent discrepancies.

Recently, the issue of redox regulation of zinc fingers has been addressed [102, 103]. Since zinc fingers contain cysteine residues, they can undergo reversible oxidation forming disulfide bridges. Oxidized zinc fingers are unable to bind zinc and therefore do not form the three-dimensional fold necessary for DNA binding. This provides a redox mechanism to regulate the activity of the zinc finger proteins. However, undesired oxidation of zinc fingers has toxic effects and may cause cancer diseases [104].

Plastocyanin

The metal ion of electron-transferring metalloproteins plays a key role in the electron transferring reaction. The electron transfer capability of these proteins is a result of the unusual geometric and electronic structures imposed on the metal ion by the protein environment [5, 105–107]. One of the major goals of the studies of electron-transferring metalloproteins has, therefore, been to determine these structures, in order to elucidate the interplay between the electronic and geometric structure of the metal site and to understand the mechanism of the electron transfer process [3, 5, 106, 108, 109].

Plastocyanin is a blue copper protein that transfers electrons from cytochrome b_6f to the chlorophyll reaction center P700 in photosystem I of the photosynthesis. The protein contains a copper ion bound to two histidines, a cysteine and a methionine at the active site. The copper ion is coordinated in a distorted tetrahedral arrangement, and it can be either in the reduced, diamagnetic Cu^{+} state or the oxidized, paramagnetic Cu^{2+} state.

The rapid and long-range electron transfer reactivity that characterizes the blue copper proteins is believed to rely on an unusual electronic structure of the metal site. Thus, the unpaired electron spin is not located solely on the paramagnetic metal ion, but is delocalized to the metal ligands. Determination of the spatial distribution of the unpaired electron spin can be obtained experimentally by X-ray absorption spectroscopy (XAS) [110, 111], ENDOR [112] and paramagnetic NMR spectroscopy [113–115], or theoretically by quantum chemical calculations [116–119]. It has been found that about 50% of the unpaired

electron spin resides on the copper, while 40% is located on the sulfur atom of the metal-coordinating cysteine [114–116].

A weak binding of the methionine sulfur to the copper ion in the blue copper proteins controls the properties of the active site. Thus, in the copper site of plastocyanin, the position of the weakly bound sulfur ensures a nearly axial geometry of the metal site, while in nitrate reductase, the geometry is more rhombic [5]. This difference in metal site geometry of the two proteins gives rise to different colors of the proteins (blue versus green) and different redox potentials [3, 5, 107]. Thus, the geometric structure of the metal site of the blue copper proteins forms the basis for a detailed understanding of the biological function of these proteins.

The geometric structure of the metal site of blue copper proteins has been determined primarily by X-ray crystallography [120] and EXAFS in the solid state, and structural changes in the metal site coordination sphere as low as 0.1 Å have been detected by combining high-resolution crystallography and EXAFS [121]. However, these structures were all determined in the solid state, while the function of metalloproteins depends on the structure and dynamics of the metal sites in solution. Therefore, detailed knowledge of the characteristics of the solution structure of the metal site is of interest.

Recently, an NMR method was presented that allows a determination of the geometric structure of the metal site in blue copper proteins in solution [122]. The method relies on a determination of the longitudinal paramagnetic relaxation enhancements, R_{1p}, of the nuclei of the ligand residues. In this context, the signal eliminating relaxation filter (SERF) experiment [123] proves valuable, because it allows determination of the paramagnetic relaxation enhancements of the nuclei close to the paramagnetic metal site, even if the NMR signals of these nuclei are broadened due to the strong electron-nucleus interaction. The experimental paramagnetic relaxation enhancements can be converted into distances using equations 3 and 4. However, if the nuclei that form the basis for the determination of the geometric structure are within 5 Å of the metal ion, the spatial electron spin distribution near the metal site must be taken into account. Thus, the distance r in equations 3 and 4 must be substituted by an effective distance parameter, r_{eff}, that depends on both the location of the nucleus relative to the metal site and the electron spin distribution. In this way, it was shown recently [122] that the geometry of the metal site can be obtained from the paramagnetic relaxation enhancements of the nuclei surrounding the metal site despite the spin distribution. Furthermore, the chemical shifts of the nuclei of the ligand residues can provide valuable information about the geometric structure of the metal site. Thus, the saturation transfer experiment allows the observation of NMR signals from protons that are as close as three bonds to the metal ion [113] despite their extreme chemical shifts and signal line widths. These chemical shifts can be converted into dihedral angles through a Karplus-like relation [113, 124] and do in general provide information about the active-site structure [125, 126]. Metal substitution in the blue copper proteins has also proved valuable. As amply demonstrated, the paramagnetic ^{1}H NMR spectra of Co^{2+}-and Ni^{2+}-substituted blue copper proteins possess hyperfine-shifted resonances which are much sharper than their counterparts in the Cu^{2+} proteins [127, 128]. These sharper signals can be assigned, and detailed analyses of the active-site structure of several blue copper proteins have been carried out [127–132].

In the case of plastocyanin from *Anabaena variabilis* (*A. v.*), the solution structure of the metal site was determined [122] by including the effective distances derived from the paramagnetic NMR relaxation as restraints in a conventional NMR structure determination, together with the inter-proton distance restraints (NOEs) and the dihedral angle restraints (scalar nuclear spin-spin couplings) normally used for structure determination of proteins by NMR [20]. The paramagnetic relaxation is thus used to restrain the geometry of the metal site, while the conventional restraints determine the overall protein matrix. Figure 6 shows the first coordination sphere of the copper site in *A. variabilis* plastocyanin obtained in solution by the paramagnetic NMR method [114, 122]. In Table 1, the bond lengths and bond angles obtained in solution by the paramagnetic NMR approach are compared with the corresponding bond lengths and bond angles observed in the crystal structure. In general, there is a good agreement between the bond lengths obtained in the solid phase by X-ray crystallography and in solution by NMR. Small differences in the bond angles are observed, in particular the bond angles that involve the axially and weakly bound methionine sulfur. Thus, it seems that the binding of the methionine sulfur goes from nearly perfectly axial in the solution state to slightly more rhombic in the crystal phase. However, this difference could also be due to dynamics of the weakly bound methionine ligand in solution.

α-Synuclein

Metal ions interact with many pathogenic proteins. This is true, for example, for the proteins involved in a number of neurodegenerative diseases such as Alzheimer, Parkinson and prion diseases. Many of these

Table 1. Comparison of bond lengths and dihedral angles in the metal site of plastocyanin from *Anabaena variabilis*

	NMR[1]	X-ray[2]	X-ray[3]
Bond lengths (Å)			
$Cu–N_{H39}$	1.94 ± 0.03	2.07	1.99
$Cu–S_{C89}$	2.12 ± 0.09	2.13	2.23
$Cu–N_{H92}$	1.98 ± 0.03	2.10	2.07
$Cu–S_{M97}$	2.80 ± 0.12	2.77	2.72
Bond angles (deg.)			
$N_{H39}–Cu–S_{C89}$	118 ± 6	132	128
$N_{H39}–Cu–N_{H92}$	116 ± 9	96	101
$N_{H39}–Cu–S_{M97}$	106 ± 15	90	93
$S_{C89}–Cu–N_{H92}$	114 ± 6	120	117
$S_{C89}–Cu–S_{M97}$	88 ± 6	110	109
$N_{H92}–Cu–S_{M97}$	105 ± 6	101	102
Geometric distances (Å)			
Cu–{NNS}[4]	0.35 ± 0.07	0.41	0.45

[1] The average of the ten structures with lowest energy shown in Figure 6. The uncertainties are the root mean square deviations (RMSD) of the bond lengths and angles calculated for the structures in Figure 6.[2] Angles and distances from the crystal structure of plastocyanin from *A. v.* at pH 8.0 (PDB: 2GIM, model no. 1).
[3] PDB: 2GIM, model no. 2.
[4] The distance from the copper ion to the plane formed by His39 Nδ1, His92 Nδ1, and Cys89 Sγ. The positive value indicates that the copper atom is located toward the Met97 Sδ ligand from the NNS plane.

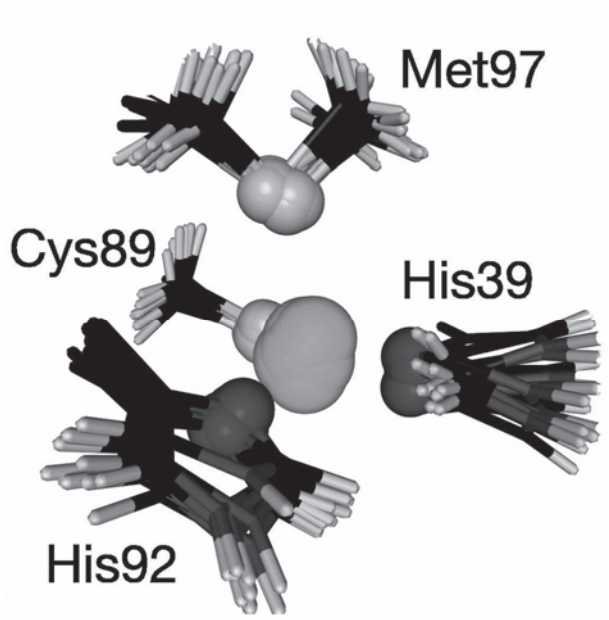

Figure 6. The first coordination sphere of the copper site of *Anabaena variabilis* plastocyanin. The superimposed structures are the ten structures with lowest energy determined by paramagnetic NMR in solution [122]. The RMSD of the ligand atoms of the ten structures is 0.17 Å. The figure was created with MOLMOL [182]. Reproduced with permission from Proc. Natl. Acad. Sci. USA (2006), vol. 103, pp. 1738–1743. Copyright 2006 Natl. Acad. Sci. USA.

proteins have a tendency to misfold, aggregate and form solid deposits, which can cause neuronal damage [133]. The interaction with the metal ions may either stabilize the proteins in their normal form, thus preventing the pathogenesis, or it may stimulate the misfolding and aggregation, giving rise to the disease. Studies of the metal-protein interactions in such systems are challenging, and elucidation of the function of the metal ion is often difficult. Recently, Gaggelli et al. [12] published an excellent review on copper homeostasis and neurodenerative disorders.

α-Synuclein is a 140-amino acid protein consisting of the amphipathic N-terminus (residues 1–60), the hydrophobic self-aggregating non-Aβ component (NAC) (residues 61–95) and the acidic C-terminus (residues 96–140). The protein has no significant secondary structure in solution; however, long-range contacts between the N-terminus and the C-terminus of the protein have been identified [134–136]. Aggregation and subsequent fibrillation of this protein is known to be involved in Parkinson disease, and it has been found that some transition metal ions, in particular Cu^{2+}, accelerate α-synuclein fibril formation in vitro [137–139].

Recently, detailed investigations of the interaction between α-synuclein and Cu^{2+} were carried out in order to understand the mechanism of aggregation and subsequent fibrillation [140, 141]. NMR spectroscopy was used to provide a per-residue basis for studying the interaction between the protein and the paramagnetic Cu^{2+} ion. Thus, the NMR signals of nuclei spatially close to the Cu^{2+}-binding sites will broaden due to an increased R_2 relaxation caused by the interactions with the unpaired electron of the metal ion. Figure 7 (upper panel) shows the decrease in signal intensity upon addition of Cu^{2+} (20 μM) to a sample of α-synuclein (100 μM) at pH 6.5 in a ^{1}H-^{15}N correlated spectrum (HSQC) as function of the residue number. The largest decrease in signal intensity is observed around H50, which is therefore identified as the major site of interaction. Upon further increase of the Cu^{2+} concentration (40 μM), two additional sites of interaction are observed, one involving an acidic patch at the C-terminus consisting of D119, D121, N122 and E123, and one involving the N-terminus of the protein [140, 141] (see Fig. 7, middle panel). The lower panel of Figure 7 shows the intensity profile for 100 μM α-synuclein and 20 μM Cu^{2+} at a lower pH value, namely pH 5.0. The binding sites in α-synuclein have different pK_a values (see Table 2), which result in an almost complete protonation of H50 and the N-terminal NH_2 group at pH

5.0, while the acidic patch at the C-terminus is mostly deprotonated. Therefore, increased binding of Cu^{2+} to the acidic patch at the C-terminus of α-synuclein is observed at lower pH values. Besides the three major interaction sites for Cu^{2+}, several carboxylate sites on the protein surface with significantly lower binding affinity could be identified [140, 141]. Other transition metal ions, such as Fe^{2+}, Mn^{2+}, Ni^{2+} and Co^{2+}, were also found to interact with α-synuclein, although the interaction is weaker and less specific. These metal ions interact mainly with the C-terminus of α-synuclein, the major interaction site being the residue D121 [139].

Table 2. Typical pK_a ranges of ionizable groups in proteins [180].

Ionizable group	Typical pK_a range
C-terminus	3.5–4.0
N-terminus	8.0–9.0
Asp/Glu	4.0–4.8
His	6.5–7.4
Cys	8.5–9.0
Tyr	9.5–10.5
Lys	9.8–10.4
Arg	≈12

Nevertheless, it is unclear how the binding of Cu^{2+} and other transition metal ions promote aggregation of α-synuclein. Exposure of the highly hydrophobic NAC domain to the solvent is believed to trigger the aggregation [142, 143]. However, as judged from the NMR chemical shifts, the overall conformation of the protein does not change upon Cu^{2+} binding [140]. Furthermore, the binding of Cu^{2+} to α-synuclein does not induce or break any long-range interactions [141] that could lead to the exposure of the NAC domain. A reason for the enhanced fibril formation of α-synuclein in the presence of Cu^{2+} could be that each Cu^{2+} ion binds several α-synuclein molecules.

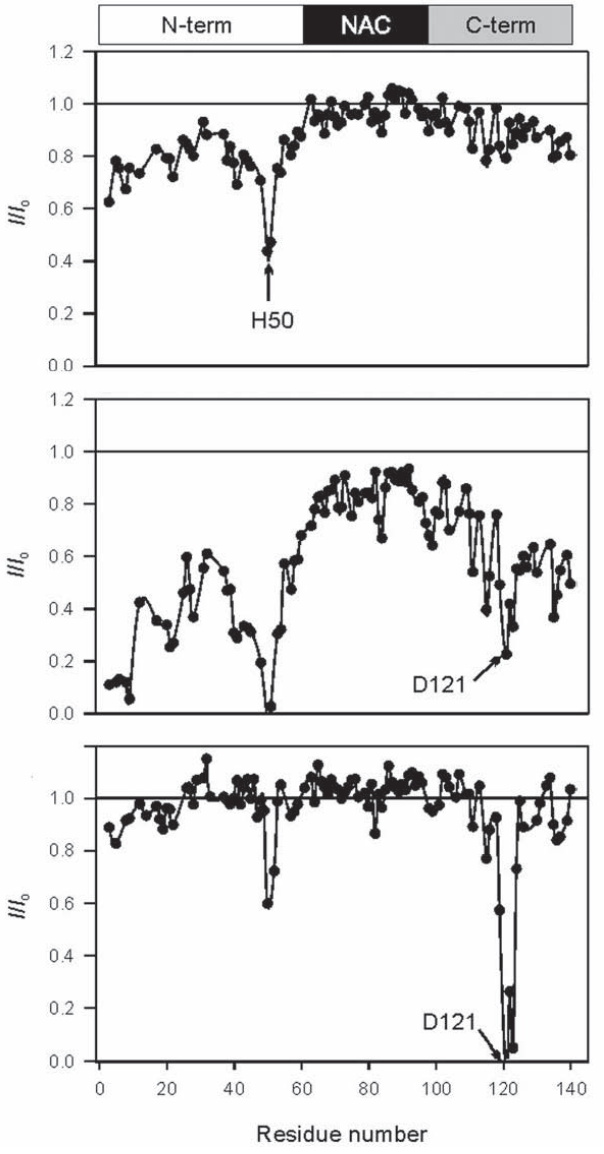

Figure 7. Intensity profiles of the ^{1}H-^{15}N HSQC NMR signals of 100 μM α-synuclein. I_0 is the intensity in the HSQC spectrum recorded without the addition of the paramagnetic Cu^{2+} ions. I is the intensity upon addition of 20 μM Cu^{2+} at pH 6.5 (upper panel), 40 μM Cu^{2+} at pH 6.5 (middle panel) and 20 μM Cu^{2+} at pH 5.0 (lower panel). Reproduced with permission from Proc. Natl. Acad. Sci. USA (2005), vol. 102, pp. 4294–4299. Copyright 2005 Natl. Acad. Sci. USA.

Prion proteins

Prions are glycoproteins that cause transmissible and genetic neurodegenerative diseases, including scrapie and bovine spongiform encephalopathy (BSE) of animals and Creutzfeldt-Jakob (CJD) and Gerstmann-Straussler-Scheinker (GSS) diseases of humans [144]. The key event in the pathogenesis of the prion diseases is the conversion of a normal cellular prion protein, PrP^{C}, to an abnormal isoform, PrP^{Sc} that is protease resistant and possibly the agent of infection [144]. The two isoforms have identical primary structures and differ only in chain conformation and state of assembly. PrP^{C} is a proteinase K (PK)-sensitive monomer with about 40 % α-structure and almost no β-structure, while PrP^{Sc} is an assembled multimer characterized by enhanced resistance toward PK digestion and containing about 40 % β-structure and about 30 % α structure [145, 146].

Although the function of PrP^{C} is still a subject of debate, there is ample evidence for the biological relevance of the copper binding. Thus, it was found that Cu-PrP^{C} has superoxide dismutase activity [147, 148], and it was suggested that a causative factor for

the prion disease could be a loss or an alteration of this activity and its antioxidant function [149]. It has also been proposed that PrP^C has a protective role by binding Cu^{2+} in a redox-inactive state [150] and that PrP^C functions as a Cu^{2+} transporter by binding Cu^{2+} ions from the extracellular medium under physiological conditions, then releasing the metal upon exposure to acidic pH in endosomes or secondary lysosomes [151–153].

To gain further insight into the role of Cu^{2+} for the function of prions, the metal binding and the structure of the binding site(s) have been investigated by NMR. The prion protein has a large N-terminal tail that contains four successive copies of the highly conserved octapeptide repeat sequence PHGGGWGQ between residues 60 and 91 (Fig. 8). Structural analysis of the prion protein in solution revealed two domains: a globular C-terminal part (121–231) of PrP^C, the structure of which has been determined by NMR spectroscopy [154–157], and the N-terminal part, which is unstructured in the absence of divalent metal ions. The octarepeat region binds up to four Cu^{2+} ions in a cooperative manner [151, 158–160] and with high selectivity [151, 153, 161–166].

As in the case of α-synuclein (see above), the location of the Cu^{2+}-binding sites in the PrP^C fragment 91–231 was identified by measuring the transverse paramagnetic relaxation enhancement, R_{2p}, given by the increase in the NMR linewidths, and the reduction in signal intensities in a ^1H–^{15}N HSQC spectrum as function of an increasing concentration of the paramagnetic Cu^{2+} ion [166] (Fig. 9). Thus, it was found that residues 94–98, 108–114, 135–136, and 153–159 exhibit significant differential alteration of resonances, indicating copper binding. In addition, the peaks that arise from the backbone amide resonances close to the binding site of the paramagnetic ion, for example, H96 and H111, exhibit significant broadening. More recently, Gaggelli et al. [167] used longitudinal paramagnetic NMR relaxation enhancements, R_{1p}, to study the binding of Cu^{2+} to the PrP^C fragment 106–126 and found that Cu^{2+} binds to His111 and the N-terminal end of the peptide. Moreover, the relaxation enhancements provided precise information about the geometric structure of the binding site (Fig. 10).

Nevertheless, the role of copper in the pathogenesis of prion diseases seems rather complex. Depending on circumstances, Cu^{2+} may have opposing effects on the development of prion diseases. On the one hand, Cu^{2+} inhibits the conversion of the prion protein into a disease-specific conformation, such as amyloid fibrils [168]. On the other, Cu^{2+} can stabilize PrP^{Sc} by converting it into a more proteolytically resistant form by enhancing the PK resistance of preformed fibrils and initiating aggregation of the amyloid fibrils into large clumps [168], which eventually reduces the rate of PrP^{Sc} clearance. Thus, the development of prion diseases may be controlled by a fine dynamic balance between the rates of PrP^{Sc} formation versus its clearance [169, 170]

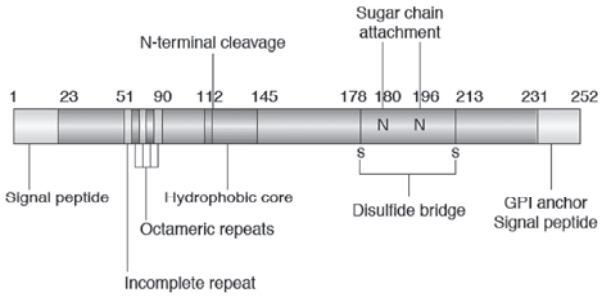

Figure 8. The primary structure of the mouse prion protein. The protein is anchored to the cell membrane by a glycosylphosphatidylinositol (GPI) anchor. The complete octameric repeats can bind up to four copper atoms; most mammals also have an incomplete repeat located upstream of this. Reproduced with permission from Trends Neurosci. (2001), vol. 24, pp. 85–90. Copyright 2001 Elsevier.

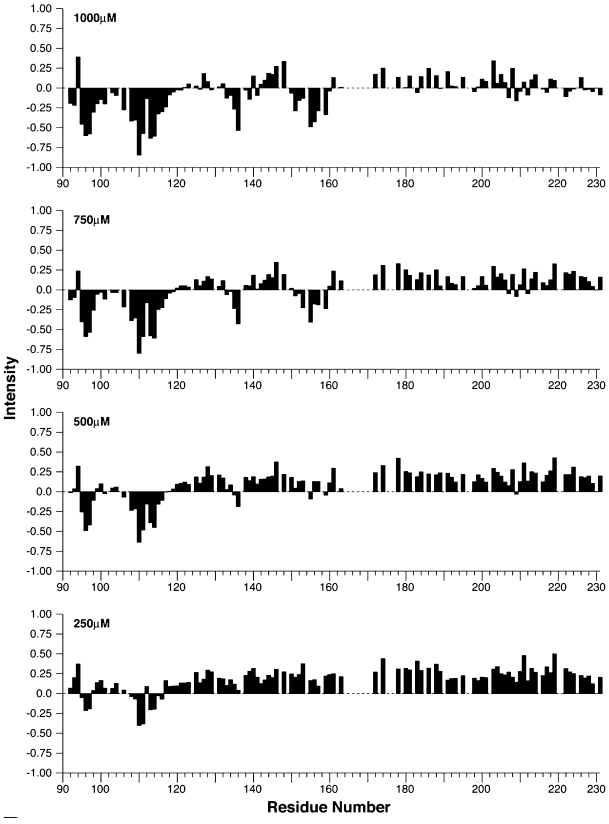

Figure 9. NMR signal intensity versus residue number. HSQC peak intensities shown sequentially at 250, 500, 750 and 1000 μM $CuSO_4$ relative to 0 μM $CuSO_4$; showing the effects of addition of Cu^{2+} to the human PrP91-231. Reproduced with permission from Proc. Natl. Acad. Sci. USA (2001), vol. 98, pp. 8531–8535. Copyright 2001 Natl. Acad. Sci. USA.

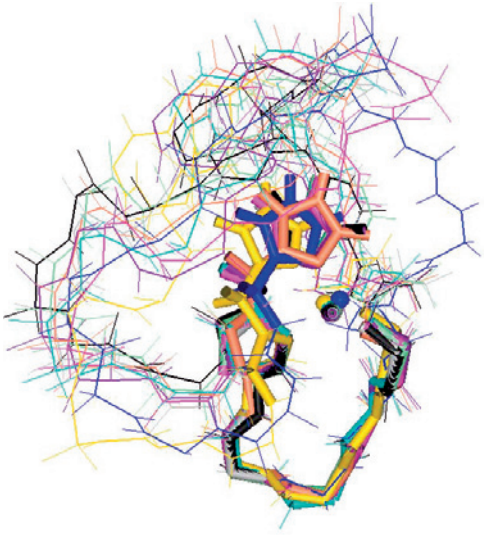

Figure 10. Superposition of Cu^{2+}–PrP106-126 structures obtained from experimental data (blue) from energy minimization (yellow) and from molecular dynamics calculations (orange). All the other colored structures represent the snapshots from molecular dynamics. The figure was created with MOLMOL [182]. Reproduced with permission from J. Am. Chem. Soc. (2005), vol. 127, pp. 996–1006. Copyright 2005 Am. Chem. Soc.

and, therefore, the final outcome of the copper-induced effects on the progression of the prion diseases may not be straightforward.

Prion proteins also bind other divalent metal ions. Thus, Ni^{2+}, Zn^{2+} or Mn^{2+} bind to PrP^C [147, 166, 167, 171–175] although considerably more weakly than Cu^{2+} [166]. In particular, the binding of Mn^{2+} has been investigated in detail since it might be associated with the transformation of the prion proteins from the normal to the abnormal form. Indeed, *in vitro* studies [148, 173] suggested that the interaction with Mn^{2+} causes conversion of PrP^C to a protease-resistant form, PrP^{res}, probably by binding to the octarepeat region (residues 60–91). In contrast to these findings, Garnett et al. [159] did not observe any Mn^{2+} binding to the octarepeat region of full-length PrP^C. Tsenkova et al. [176] suggested that Mn^{2+} may lead to fibrillation, while Bocharova et al. [168] failed to detect any fibrillation effect from Mn^{2+} on full-length PrP^C. In their detailed paramagnetic NMR relaxation study, Gaggelli et al. [167] showed that the PrP^C106–126 fragment strongly binds Mn^{2+}, although the observed paramagnetic relaxation enhancements, R_{1p}, in the case of Mn^{2+} were mostly dependent on the exchange lifetimes and, therefore, did not contain quantitative structural information. Nevertheless, the authors found that the two metal ions bind to the peptide in two different regions. Thus, the N-terminal region is affected by Cu^{2+}, while Mn^{2+} binds to the C-terminal G126 carboxylate and the preceding carbonyl residues, resulting in different coordination modes for the two metal complexes.

Taken together, the importance of Cu^{2+} and other divalent metal ions for the function of prions has been clearly demonstrated by numerous studies. However, the studies also illustrate the complexity of the interaction of copper with prion proteins and, thus, the complexity of the effect of copper on the development of prion diseases.

Thioredoxin

As discussed above, the metal ion binding of α-synuclein and prion proteins is important for the biological function of the proteins. However, in both cases, the location and characteristics of the metal binding site are less well defined, and the precise function of the metal ions is still unknown. A similar uncertainty or lack of insight applies to other metal-dependent proteins, for example tRNA synthetases. In the studies of α-synuclein and prion proteins, as well as in other studies [140, 141, 166, 167, 177, 178], the location of the Cu^{2+} ions was identified through the paramagnetic broadening (R_{2p}) of the NMR signals of the nuclei spatially close to the metal-binding sites. However, this approach does not provide information that is sufficiently detailed for a precise determination of the location and the characteristics of the metal-binding sites. Moreover, if the occupancies of some of the binding sites are low, the line broadening may be less significant or it may be obscured by other effects. Recently, an NMR approach was presented [62] that, in principle, alleviates these shortcomings. The approach relies on the structure of the protein and on a determination of the longitudinal paramagnetic relaxation enhancements, R_{1p}, of a large number of nuclei in the protein. Thus, by using the distance information provided by the R_{1p} rates, all binding sites on the protein surface can be located [61, 62]. A simultaneous determination of the location of the binding sites and the occupancies can be obtained by including in the analysis the pH dependence of the paramagnetic relaxation rates for a single concentration of the paramagnetic metal ion. This was demonstrated for *Escherichia coli* thioredoxin using Ni^{2+} as the paramagnetic metal ion [62]. As multifunctional proteins, thioredoxins participate in many different redox reactions through the reversible oxidation of two free thiol groups to a disulfide bridge at the active site. Thus, for example, thioredoxins catalyze the degradation of insulin and they are implicated in the regulation of enzyme activities [179]. However, no functional importance of metal ion binding to thioredoxin has been reported.

In the study, a total of five distinct Ni^{2+}-binding sites were identified on the surface of thioredoxin. Side

chain carboxylate groups constitute four of the binding sites, while the N-terminus of the protein provides the fifth binding site (see Fig. 11). The occupancies of the individual binding sites were determined from the combined results of a series of pH and Ni^{2+} titration experiments. The approach relies on the fact that the binding of metal ions to a protein is highly pH dependent and is mainly controlled by the pK_a values of the ligands. Table 2 shows the typical pK_a ranges of ionizable groups in proteins. In the pH titration experiments, the observed longitudinal relaxation rates of the amide protons were measured as a function of the pH for a constant protein and Ni^{2+} concentration of 1.0 mM. If Ni^{2+} binds to the protein, enhanced nuclear relaxation rates are observed. Figure 12 shows the appearance of a pH titration curve for the amide proton of G21. This amide proton is affected both by the carboxylate binding site at D20 and indirectly by the strongest binding site located at the N-terminus of thioredoxin. Since the N-terminal binding site in thioredoxin becomes protonated before the carboxylate binding site (see Table 2), more Ni^{2+} becomes available to the carboxylate binding sites as the pH is lowered from 7.0 to approximately 5.5. Consequently, an increase in the observed longitudinal relaxation rates of the nuclei close to the carboxylate binding sites, including the D20 site, is observed as the pH is lowered. Below pH 5.5, the carboxylate binding sites becomes protonated and the relaxation rates decrease. Thus, the pH dependence of the longitudinal relaxation rate in combination with its dependence on the Ni^{2+} concentration form the basis for a simultaneous determination of the location of the binding sites and the associated binding constants. In the case of the investigated Ni^{2+}-thioredoxin interaction, it was found that for an equivalent amount of protein and Ni^{2+} (1.0 mM), the occupancies of the five binding sites in thioredoxin are S1/D2 (47%), D10 (11%), D20 (7%), D47 (3%), and E85 (2%), while 30% of the Ni^{2+} remains unbound [62].

Finally, the detection of a large number of weak metal-binding sites in thioredoxin raises the question whether they are of any biological significance. The fact that most proteins have similar low-affinity metal-binding capabilities in terms of surface-exposed carboxylate groups or histidine imidazole groups further emphasizes the significance of this question.

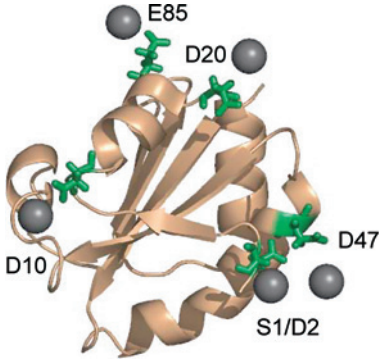

Figure 11. Ribbon model of the solution structure of thioredoxin showing the five different Ni^{2+}-binding sites on the protein surface. The carboxylate side chains are shown in green while the Ni^{2+} ions are shown in gray. The figure was created with PyMOL [181]. Reproduced with permission from Biochemistry (2005), vol. 44, pp. 11014–11023. Copyright 2005 Am. Chem. Soc.

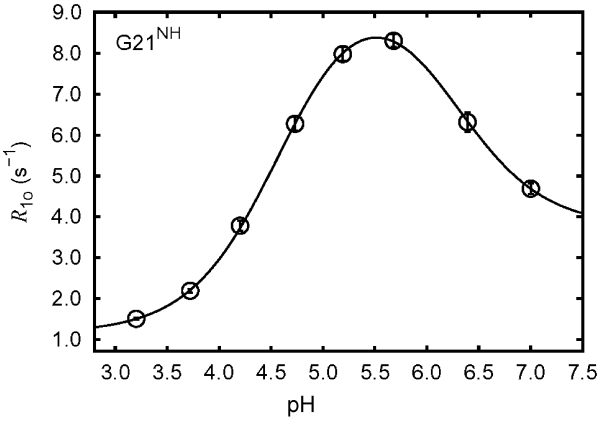

Figure 12. pH titration curve for the amide proton $G21^{NH}$ in thioredoxin. A sample of 1.0 mM protein and 1.0 mM Ni^{2+} was used. The observed longitudinal relaxation rates were measured at 11.74 T for eight different pH values in the range from 3.2 to 7.0. The relaxation rate of the amide proton $G21^{NH}$ follows a two-step titration (solid line) with pK_a values of 4.7 ± 0.1 and 6.2 ± 0.1. The curvature of the pH dependence shows that $G21^{NH}$ is affected by two or more metal-binding sites. Reproduced with permission from Biochemistry (2005), vol. 44, pp. 11014–11023. Copyright 2005 Am. Chem. Soc.

Concluding remarks

Recent studies have challenged our view of metal-protein interactions. A picture emerges that not only contains the classical metalloproteins with well-defined, highly ordered and static metal sites, as found in plastocyanin, but also includes proteins and peptides where the interactions with the metal ion are highly diverse and dynamic. Nevertheless, the indication that metal-protein interactions are involved in neurodegenerative diseases suggests that these transient interactions are of great biological relevance. Signal proteins such as calmodulin, and zinc fingers in transcription factors have well-defined binding sites, yet the metal binding is likely to be transient at *in vivo* conditions. Here, life utilizes metal ions as a part of a complicated regulatory network. To understand the mechanisms by which these proteins function, it is important to understand the interplay between the

dynamics of the protein and the binding of the metal ion.

The diversity of metal-binding sites found throughout the proteome is a great challenge to biophysics. In particular, the more transient metal-protein interactions are difficult to monitor. Within this field, NMR has a great potential. Techniques to study conventional static metal-binding sites by paramagnetic NMR are fairly well established; however, the methods are still being refined in order to improve the quality of the metal site structures of proteins in solution and to obtain information about the electronic structure of metal sites. Today, paramagnetic NMR techniques are also used to characterize weak or transient binding sites, and diamagnetic NMR relaxation studies can provide complementary information about protein motions coupled to metal binding. However, NMR cannot be the only technique used to study metal binding of proteins and peptides. X-ray crystallography, EXAFS, EPR, UV-VIS, CD, vibrational spectroscopy, mass spectrometry and other techniques, are necessary to obtain satisfactory answers.

Finally, the finding of Ni^{2+}-binding sites on the surface of thioredoxin, a protein that is not considered to utilize metal ions for its biological function in any way, raises the intriguing question: are metal-dependent proteins more common than originally thought?

Acknowledgements

We thank A. Hammershøi and J. Ulstrup for helpful discussions. This work was financially supported by the Danish Natural Science Research Council, J. No. 9400351, 51-00211, and 21-04-0519, Carlsbergfondet, J. No. 1624/40, Novo Nordisk Fonden, J. No. 2003-11-28, and Villum Kann Rasmussen Fonden, J. No. 8.12.2003. The 800 MHz spectrometer at The Danish Instrument Center for NMR Spectroscopy of Biological Macromolecules was used in some of the NMR studies reviewed here.

1 Lu, Y. and Valentine, J. S. (1997) Engineering metal-binding sites in proteins. Curr. Opin. Struct. Biol. 7, 495 – 500.
2 Gross, E. L. (1993) Plastocyanin: structure and function. Photosyn. Res. 37, 103 – 116.
3 Gray, H. B., Malmström, B. G. and Williams, R. J. P. (2000) Copper coordination in blue proteins. J. Biol. Inorg. Chem. 5, 551 – 559.
4 De Rienzo, F., Gabdoulline, R. R., Wade, R. C., Sola, M. and Menziani, M. C. (2004) Computational approaches to structural and functional analysis of plastocyanin and other blue copper proteins. Cell. Mol. Life Sci. 61, 1123 – 1142.
5 Solomon, E. I., Szilagyi, R. K., George, S. D. B. and Basumallick, L. (2004) Electronic structures of metal sites in proteins and models: contribution to function in blue copper proteins. Chem. Rev. 104, 419 – 458.
6 Párraga, G., Horvath, S. J., Eisen, A., Taylor, W. E., Hood, L., Young, E. T. and Klevit, R. E. (1988) Zinc-dependent structure of a single-finger domain of yeast ADR1. Science 241, 1489 – 1492.
7 Wilson, C. J., Apiyo, D. and Wittung-Stafshede, P. (2004) Role of cofactors in metalloprotein folding. Q. Rev. Biophys. 37, 285 – 314.
8 Shriver, D. F., Atkins, P. W., Overton, T. L., Rourke, J. P., Weller, M. T. and Armstrong, F. A. (2006) Inorganic Chemistry, 4th edition, p. 715, Oxford University Press.
9 Capozzi, F., Casadei, F. and Luchinat, C. (2006) EF-hand protein dynamics and evolution of calcium signal transduction: an NMR view. J. Biol. Inorg. Chem. 11, 949 – 962.
10 Gong, Q., Guo, Q., Tong, K.-L., Zhu, G., Wong, J. T.-F. and Xue, H. (2002) NMR analysis of bovine $tRNA^{Trp}$: conformation dependence of Mg^{2+} binding, J. Biol. Chem. 277, 20694 – 20701.
11 Zhang, C.-M., Perona, J. J. and Hou, Y.-M. (2003) Amino acid discrimination by a highly differentiated metal center of an aminoacyl-tRNA synthetase. Biochemistry 42, 10931 – 10937.
12 Gaggelli, E., Kozlowski, H., Valensin, D. and Valensin, G. (2006) Copper homeostasis and neurodegenerative disorders (Alzheimers, prion, and parkinsons diseases and amyotrophic lateral sclerosis). Chem. Rev. 106, 1995 – 2044.
13 Blundell, T. L., Dodson, G. G., Hodgkin, D. M. C. and Mercola, D. A. (1972) Insulin: the structure in crystal and its reflection in chemistry and biology. Adv. Protein Chem. 26, 279 – 402.
14 Cunningham, B. C., Mulkerrin, M. G. and Wells, J. A. (1991) Dimerization of human growth hormone by zinc. Science 253, 545 – 548.
15 Cavanagh, J., Fairbrother, W. J., Palmer III, A. G. and Skelton, N. J. (1996) Protein NMR Spectroscopy. Principles and Practice, pp. 478 – 518, Academic Press, San Diego.
16 Pervushin, K., Riek, R., Wider, G. and Wüthrich, K. (1997) Attenuated T_2 relaxation by mutual cancellation of dipole-dipole coupling and chemical shift anisotropy indicates an avenue to NMR structures of very large biological macromolecules in solution. Proc. Natl. Acad. Sci. USA. 94, 12366 – 12371.
17 Shuker, S. B., Hajduk, P. J., Meadows, R. P. and Fesik, S. W. (1996) Discovering high-affinity ligands for proteins: SAR by NMR. Science 274, 1531 – 1534.
18 Pellecchia, M., Montgomery, D. L., Stevens, S. Y., Kooi, C. W. V., Feng, H. P., Gierasch, L. M. and Zuiderweg, E. R. (2000) Structural insights into substrate binding by the molecular chaperone DnaK. Nat. Struct. Biol. 7, 298 – 303.
19 Zuiderweg, E. R. P. (2002) Mapping protein-protein interactions in solution by NMR spectroscopy. Biochemistry 41, 1 – 7.
20 Wüthrich, K. (1986) NMR of Proteins and Nucleic Acids, pp. 93 – 114. Wiley, New York.
21 Badsberg, U., Jørgensen, A. M. M., Gesmar, H., Led, J. J., Hammerstad, J. M., Jespersen, L.-L. and Ulstrup, J. (1996) Solution structure of reduced plastocyanin from the blue-green alga *Anabaena variabilis*. Biochemistry 35, 7021 – 7031.
22 Öz, G., Pountney, D. L. and Armitage, I. M. (1998) NMR spectroscopic studies of $I=1/2$ metal ions in biological systems, Biochem. Cell Biol. 76, 223 – 234.
23 Akke, M. and Chazin, W. J. (2001) An open and shut case. Nat. Struct. Biol. 8, 910 – 912.
24 Kay, L. E., Torchia, D. A. and Bax, A. (1989) Backbone dynamics of proteins as studied by ^{15}N inverse detected heteronuclear NMR spectroscopy: application to staphylococcal nuclease. Biochemistry 28, 8972 – 8979.
25 Ishima, R. and Torchia, D. A. (2000) Protein dynamics from NMR. Nat. Struct. Biol. 7, 740 – 743.
26 Palmer, A. G. (2004) NMR characterization of the dynamics of biomacromolecules. Chem. Rev. 104, 3623 – 3640.
27 Mandel, A. M., Akke, M. and Palmer, A. G. (1995) Backbone dynamics of *Escherichia coli* ribonuclease HI: correlations with structure and function in an active enzyme. J. Mol. Biol. 246, 144 – 163.
28 Kay, L. E. (2005) NMR studies of protein dynamics. J. Magn. Reson. 173, 193 – 207.

29 Boehr, D. D., Dyson, H. J. and Wright, P. E. (2006) An NMR perspective on enzyme dynamics. Chem. Rev. 106, 3055 – 3079.

30 Lipari, G. and Szabo, A. (1982) Model-free approach to the interpretation of nuclear magnetic resonance relaxation in macromolecules. 1. Theory and range of validity. J. Am. Chem. Soc. 104, 4546 – 4559.

31 Lipari, G. and Szabo, A. (1982) Model-free approach to the interpretation of nuclear magnetic resonance relaxation in macromolecules. 2. Analysis of experimental results. J. Am. Chem. Soc. 104, 4559 – 4570.

32 Carr, H. Y. and Purcell, E. M. (1954) Effects of diffusion on free precession in nuclear magnetic resonance experiments. Phys. Rev. 94, 630 – 638.

33 Meiboom, S. and Gill, D. (1958) Modified spin-echo method for measuring nuclear relaxation times. Rev. Sci. Instrum. 29, 688 – 691.

34 Palmer, A. G., Kroenke, C. D. and Loria, J. P. (2001) Nuclear magnetic resonance methods for quantifying microsecond-to-millisecond motions in biological macromolecules. Methods Enzymol. 339, 204 – 238.

35 Hass, M. A. S., Thuesen, M. H., Christensen, H. E. M. and Led, J. J. (2004) Characterization of μs-ms dynamics of proteins using a combined analysis of ^{15}N NMR relaxation and chemical shift: conformational exchange in plastocyanin induced by histidine protonations. J. Am. Chem. Soc. 126, 753 – 765.

36 Mandel, A. M., Akke, M. and Palmer, A. G. (1996) Dynamics of ribonuclease H: temperature dependence of motions on multiple time scales. Biochemistry 35, 16009 – 16023.

37 Kurland, R. J. and McGarvey, B. R. (1970) Isotropic NMR shifts in transition metal complexes: the calculation of the fermi contact and pseudocontact terms. J. Magn. Reson. 2, 286 – 301.

38 Arnesano, F., Banci, L. and Piccioli, M. (2005) NMR structures of paramagnetic metalloproteins. Q. Rev. Biophys. 38, 167 – 219.

39 Bertini, I., Luchinat, C., Parigi, G. and Pierattelli, R. (2005) NMR spectroscopy of paramagnetic metalloproteins. ChemBioChem 6, 1536 – 1549.

40 Donaldson, L. W., Skrynnikov, N. R., Choy, W.-Y., Muhandiram, D. R., Sarkar, B., Forman-Kay, J. D. and Kay, L. E. (2001) Structural characterization of proteins with an attached ATCUN motif by paramagnetic relaxation enhancement NMR spectroscopy. J. Am. Chem. Soc. 123, 9843 – 9847.

41 Gaponenko, V., Dvoretsky, A., Walsby, C., Hoffman, B. M. and Rosevear, P. R. (2000) Calculation of z-coordinates and orientational restraints using a metal binding tag. Biochemistry 39, 15217 – 15224.

42 Feeney, J., Birdsall, B., Bradbury, A. F., Biekofsky, R. R. and Bayley, P. M. (2001) Calmodulin tagging provides a general method of using lanthanide induced magnetic field orientation to observe residual dipolar couplings in proteins in solution. J. Biomol. NMR 21, 41 – 48.

43 Dvoretsky, A., Gaponenko, V. and Rosevear, P. R. (2002) Derivation of structural restraints using a thiol-reactive chelator. FEBS Lett. 528, 189 – 192.

44 Gaponenko, V., Altieri, A. S., Li, J. and Byrd, R. A. (2002) Breaking symmetry in the structure determination of (large) symmetric protein dimers. J. Biomol. NMR 24, 143 – 148.

45 Iwahara, J., Anderson, D. E., Murphy, E. C. and Clore, G. M. (2003) EDTA-derivatized deoxythymidine as a tool for rapid determination of protein binding polarity to DNA by intermolecular paramagnetic relaxation enhancement. J. Am. Chem. Soc. 125, 6634 – 6635.

46 Wöhnert, J., Franz, K. J., Nitz, M., Imperiali, B. and Schwalbe, H. (2003) Protein alignment by a coexpressed lanthanide-binding tag for the measurement of residual dipolar couplings. J. Am. Chem. Soc. 125, 13338 – 13339.

47 Gaponenko, V., Sarma, S. P., Altieri, A. S., Horita, D. A., Li, J. and Byrd, R. A. (2004) Improving the accuracy of NMR structures of large proteins using pseuducontact shifts as long-range restraints. J. Biomol. NMR 28, 205 – 212.

48 Ikegami, T., Verdier, L., Sakhaii, P., Grimme, S., Pescatore, B., Saxena, K., Fiebig, K. M. and Griesinger, C. (2004) Novel techniques for weak alignment of proteins in solution using chemical tags coordinating lanthanide ions. J. Biomol. NMR 29, 339 – 349.

49 Pintacuda, G., Moshref, A., Leonchiks, A., Sharipo, A. and Otting, G. (2004) Site-specific labelling with a metal chelator for protein-structure refinement. J. Biomol. NMR 29, 351 – 361.

50 Prudêncio, M., Rohovec, J., Peters, J. A., Tocheva, E., Boulanger, M. J., Murphy, M. E. P., Hupkes, H.-J., Kosters, W., Impagliazzo, A. and Ubbink, M. (2004) A caged lanthanide complex as a paramagnetic shift agent for protein NMR. Chem. Eur. J. 10, 3252 – 3260.

51 Solomon, I. (1955) Relaxation processes in a system of two spins. Phys. Rev. 99, 559 – 565.

52 Mispelter, J., Momenteau, M. and Lhoste, J.-M. (1993) Heteronuclear magnetic resonance: applications to biological and related paramagnetic molecules. Biol. Magn. Res. 12, 299 – 355.

53 Jensen, M. R. and Led, J. J. (2004) Determination of the electron relaxation rates in paramagnetic metal complexes: applicability of available NMR methods. J. Magn. Reson. 167, 169 – 177.

54 Bertini, I., Lee, Y.-M., Luchinat, C., Piccioli, M. and Poggi, L. (2001) Locating the metal ion in calcium-binding proteins by using cerium(III) as a probe. ChemBioChem 2, 550 – 558.

55 Babini, E., Bertini, I., Capozzi, F., Felli, I. C., Lelli, M. and Luchinat, C. (2004) Direct carbon detection in paramagnetic metalloproteins to further exploit pseudocontact shift restraints. J. Am. Chem. Soc. 126, 10496 – 10497.

56 Balayssac, S., Bertini, I., Luchinat, C., Parigi, G. and Piccioli, M. (2006) ^{13}C direct detected nmr increases the detectability of residual dipolar couplings. J. Am. Chem. Soc. 128, 15042 – 15043.

57 Bertini, I., Felli, I. C., Gonnelli, L., Pierattelli, R., Spyranti, Z. and Spyroulias, G. A. (2006) Mapping protein-protein interaction by ^{13}C-detected heteronuclear NMR spectroscopy. J. Biomol. NMR 36, 111 – 122.

58 Ubbink, M., Worrall, J. A. R., Canters, G. W., Groenen, E. J. J. and Huber, M. (2002) Paramagnetic resonance of biological metal centers. Annu. Rev. Biophys. Struct. 31, 393 – 422.

59 Goldfarb, D. and Arieli, D. (2004) Spin distribution and the location of protons in paramagnetic proteins. Annu. Rev. Biophys. Biomol. Struct. 33, 441 – 468.

60 McLaughlin, A. C. and Leigh, J. S. (1973) Relaxation times in systems with chemical exchange: approximate solutions for the nondilute case. J. Magn. Res. 9, 296 – 304.

61 Aime, S., D'Amelio, N., Fragai, M., Lee, Y.-M., Luchinat, C., Terreno, E. and Valensin, G. (2002) A paramagnetic probe to localize residues next to carboxylates on protein surfaces. J. Biol. Inorg. Chem. 7, 617 – 622.

62 Jensen, M. R., Petersen, G., Lauritzen, C., Pedersen, J. and Led, J. J. (2005) Metal binding sites in proteins: identification and characterization by paramagnetic NMR relaxation. Biochemistry 44, 11014 – 11023.

63 Bertini, I., Luchinat, C. and Parigi, G. (2001) Solution NMR of Paramagnetic Molecules. Applications to Metallobiomolecules and Models, p. 84 – 85. Elsevier, Amsterdam.

64 Felli, I. C., Desvaux, H. and Bodenhausen, G. (1998) Local mobility of ^{15}N labeled biomolecules characterized through cross-correlation rates: applications to paramagnetic proteins. J. Biomol. NMR 12, 509 – 521.

65 Bertini, I., Bryant, D. A., Ciurli, S., Dikiy, A., Fernández, C. O., Luchinat, C., Safarov, N., Vila, A. J. and Zhao, J. (2001) Backbone dynamics of plastocyanin in both oxidation states: solution structure of the reduced form and comparison with the oxidized state. J. Biol. Chem. 276, 47217 – 47226.

66 Head, J. F., Inouye, S., Teranishi, K. and Shimomura, O. (2000) The crystal structure of the photoprotein aequorin at 2.3 Ångström resolution. Nature 405, 372 – 376.
67 Ohashi, W., Inouye, S., Yamazaki, T. and Hirota, H. (2005) NMR analysis of the Mg^{2+}-binding properties of aequorin, a Ca^{2+}-binding photoprotein. J. Biochem. 138, 613 – 620.
68 Crivici, A. and Ikura, M. (1995) Molecular and structural basis of target recognition by calmodulin. Annu. Rev. Biophys. Biomol. Struct. 24, 85 – 116.
69 Ikura, M. (1996) Calcium binding and conformational response in EF-hand proteins. Trends Biochem. Sci. 21, 14 – 17.
70 Barbato, G., Ikura, M., Kay, L. E., Pastor, R. W. and Bax, A. (1992) Backbone dynamics of calmodulin studied by N-15 relaxation using inverse detected two-dimensional NMR spectroscopy – the central helix is flexible. Biochemistry 31, 5269 – 5278.
71 Strynadka, N. C. J. and James, M. N. G. (1989) Crystal structures of the helix-loop-helix calcium binding proteins. Annu. Rev. Biochem. 58, 951 – 998.
72 Babu, Y. S., Sack, J. S. and Greenhough, T. J. and Bugg, C. E., Means, A. R. and Cook, W. J. (1985) Three-Dimensional structure of calmodulin. Nature 315, 37 – 40.
73 Kretsinger, R. H., Rudnick, S. E. and Weissman, L. J. (1986) Crystal structure of calmodulin. J. Inorg. Biochem. 28, 289 – 302.
74 Babu, Y. S., Bugg, C. E. and Cook, W. J. (1988) Structure of calmodulin refined at 2.2 Å resolution. J. Mol. Biol. 204, 191 – 204.
75 Zhang, M., Tanaka, T. and Ikura, M. (1995) Calcium-induced conformational transition revealed by the solution structure of apo calmodulin. Nat. Struct. Biol. 2, 758 – 767.
76 Kuboniwa, H., Tjandra, N., Grzesiek, S., Ren, H., Klee, C. B. and Bax, A. (1995) Solution structure of calcium-free calmodulin. Nat. Struct. Biol. 2, 768 – 776.
77 Finn, B. E., Evenäs, J., Drakenberg, T., Waltho, J. P., Thulin, E. and Forsén, S. (1995) Calcium-induced structural changes and domain autonomy in calmodulin. Nat. Struct. Biol. 2, 777 – 783.
78 Evenäs, J., Forsén, S., Malmendal, A. and Akke, M. (1999) Backbone dynamics and energetics of a calmodulin domain mutant exchanging between closed and open conformations. J. Mol. Biol. 289, 603 – 617.
79 Malmendal, A., Evenäs, J., Forsén, S. and Akke, M. (1999) Structural dynamics in the C-terminal domain of calmodulin at low calcium levels. J. Mol. Biol. 293, 883 – 899.
80 Evenäs, J., Malmendal, A. and Akke, M. (2001) Dynamics of the transition between open and closed conformations in a calmodulin C-terminal domain mutant. Structure 9, 185 – 195.
81 Linse, S., Helmersson, A. and Forsén, S. (1991) Calcium-binding to calmodulin and its globular domains. J. Biol. Chem. 266, 8050 – 8054.
82 Evenäs, J., Thulin, E., Malmendal, A., Forsén, S. and Carlström, G. (1997) NMR studies of the E140Q mutant of the carboxy-terminal domain of calmodulin reveal global conformational exchange in the Ca^{2+}-saturated state. Biochemistry 36, 3448 – 3457.
83 Evenäs, J., Malmendal, A., Thulin, E., Carlström, G. and Forsén, S. (1998) Ca^{2+} binding and conformational changes in a calmodulin domain. Biochemistry 37, 13744 – 13754.
84 Tjandra, N., Kuboniwa, H., Ren, H. and Bax, A. (1995) Rotational dynamics of calcium-free calmodulin studied by ^{15}N NMR relaxation measurements. Eur. J. Biochem. 230, 1014 – 1024.
85 Malmendal, A., Linse, S., Evenäs, J., Forsén, S. and Drakenberg, T. (1999) Battle for the EF-hands: magnesium-calcium interference in calmodulin. Biochemistry 38, 11844 – 11850.
86 Malmendal, A., Evenäs, J., Thulin, E., Gippert, G. P., Drakenberg, T. and Forsén, S. (1998) When size is important: accommodation of magnesium in a calcium binding regulatory domain. J. Biol. Chem. 273, 28994 – 29001.
87 Wittung-Stafshede, P. (2004) Role of cofactors in folding of the blue-copper protein azurin. Inorg. Chem. 43, 7926 – 7933.
88 Miller, J., McLachlan, A. D. and Klug, A. (1985) Repetitive zinc-binding domains in the protein transcription factor IIIA from *Xenopus* oocytes. EMBO J. 4, 1609 – 1614.
89 Berg, J. M. and Godwin, H. A. (1997) Lessons from zinc-binding peptides. Annu. Rev. Biophys. Biomol. Struct. 26, 357 – 371.
90 Cox, E. H. and McLendon, G. L. (2000) Zinc-dependent protein folding. Curr. Opin. Chem. Biol. 4, 162 – 165.
91 Diakun, G. P., Fairall, L. and Klug, A. (1986) EXAFS study of the zinc-binding sites in the protein transcription factor IIIA. Nature 324, 698 – 699.
92 Lee, M. S., Gippert, G. P., Soman, K. V., Case, D. A. and Wright, P. E. (1989) Three-dimensional solution structure of a single zinc finger DNA-binding domain. Science 245, 635 – 637.
93 Nolte, R. T., Conlin, R. M., Harrison, S. C. and Brown, R. S. (1998) Differing roles for zinc fingers in DNA recognition: structure of a six-finger transcription factor IIIA complex. Proc. Natl. Acad. Sci. USA 95, 2938 – 2943.
94 Laity, J. H., Lee, B. M. and Wright, P. E. (2001) Zinc finger proteins: new insights into structural and functional diversity. Curr. Opin. Struct. Biol. 11, 39 – 46.
95 Andreini, C., Banci, L. and Bertini, I. and Rosato, A. (2006) Counting the zinc-proteins encoded in the human genome. J. Proteome Res. 5, 196 – 201.
96 Klug, A. and Schwabe, J. W. R. (1995) Zinc fingers. FASEB J. 9, 597 – 604.
97 Frankel, A. D., Berg, J. M. and Pabo, C. O. (1987) Metal-dependent folding of a single zinc finger from transcription factor IIIA. Proc. Natl. Acad. Sci. USA 84, 4841 – 4845.
98 Miura, T., Satoh, T. and Takeuchi, H. (1998) Role of metal-ligand coordination in the folding pathway of zinc finger peptides. Biochim. Biophys. Acta 1384, 171 – 179.
99 Ghosh, M., Elsby, L. M., Mal, T. K., Gooding, J. M., Roberts, S. G. E. and Ikura, M. (2004) Probing Zn^{2+} binding effects on the zinc-ribbon of human general transcription factor TFIIB. Biochem. J. 378, 317 – 324.
100 Giedroc, D. P., Chen, X., Pennella, M. A. and LiWang, A. C. (2001) Conformational heterogeneity in the C-terminal zinc fingers of human MTF-1. J. Biol. Chem. 276, 42322 – 42332.
101 Potter, B. M., Feng, L. S., Parasuram, P. P., Matskevich, V. A., Wilson, J. A., Andrews, G. K. and Laity, J. H. (2005) The six zinc fingers of metal-responsive element binding transcription factor-1 form stable and quasi-ordered structures with relatively small differences in zinc affinities. J. Biol. Chem. 280, 28529 – 28540.
102 Wu, X., Bishopric, N. H., Discher, D. J., Murphy, B. J. and Webster, K. A. (1996) Physical and functional sensitivity of zinc finger transcription factors to redox change. Mol. Cell. Biol. 16, 1035 – 1046.
103 Baldwin, M. A. and Benz, C. C. (2002) Redox control of zinc finger proteins. Methods Enzymol. 353, 54 – 69.
104 Witkiewicz-Kucharczyk, A. and Bal, W. (2006) Damage of zinc fingers in DNA repair proteins: a novel molecular mechanism in carcinogenesis. Toxicology Lett. 162, 29 – 42.
105 Solomon, E. I. and Lowery, M. D. (1993) Electronic structure contributions to function in bioinorganic chemistry. Science 259, 1575 – 1581.
106 Randall, D. W., Gamelin, D. R., LaCroix, L. B. and Solomon, E. I. (2000) Electronic structure contributions to electron transfer in blue Cu and Cu-A. J. Biol. Inorg. Chem. 5, 16 – 29.
107 Solomon, E. I. (2006) Spectroscopic methods in bioinorganic chemistry: blue to green to red copper sites. Inorg. Chem. 45, 8012 – 8025.
108 De Kerpel, J. O. A. and Ryde, U. (1999) Protein strain in blue copper proteins studied by free energy pertubation. Proteins: Structure, Function, and Genetics 36, 157 – 174.
109 Ryde, U., Olsson, M. H. M., Roos, B. O., De Kerpel, J. O. A. and Pierloot, K. (2000) On the role of strain in blue copper proteins, J. Biol. Inorg. Chem. 5, 565 – 574.
110 George, S. J., Lowery, M. D., Solomon, E. I. and Cramer, S. P. (1993) Copper L-edge spectral studies: a direct experimental

probe of the ground-state covalency in the blue copper site in plastocyanin. J. Am. Chem. Soc. 115, 2968 – 2969.
111 Shadle, S. E., Penner-Hahn, J. E., Schugar, H. J., Hedman, B., Hodgson, K. O. and Solomon, E. I. (1993) X-ray absorption spectroscopic studies of the blue copper site: metal and ligand K-edge studies to probe the origin of the EPR hyperfine splitting in plastocyanin. J. Am. Chem. Soc. 115, 767 – 776.
112 Werst, M. M., Davoust, C. E. and Hoffman, B. M. (1991) Ligand spin densities in blue copper proteins by Q-band ^{1}H and ^{14}N ENDOR spectroscopy. J. Am. Chem. Soc. 113, 1533 – 1538.
113 Bertini, I., Ciurli, S., Dikiy, A., Gasanov, R., Luchinat, C., Martini, G. and Safarov, N. (1999) High-field NMR studies of oxidized blue copper proteins: the case of spinach plastocyanin. J. Am. Chem. Soc. 121, 2037 – 2046.
114 Hansen, D. F. and Led, J. J. (2004) Mapping the electronic structure of the blue copper site in plastocyanin by NMR relaxation. J. Am. Chem. Soc. 126, 1247 – 1252.
115 Hansen, D. F., Gorelsky, S. I., Sarangi, R., Hodgson, K. O., Hedman, B., Christensen, H. E. M., Solomon, E. I. and Led, J. J. (2006) Reinvestigation of the method used to map the electronic structure of blue copper proteins by NMR relaxation. J. Biol. Inorg. Chem. 11, 277 – 285.
116 Penfield, K. W., Gewirth, A. A. and Solomon, E. I. (1985) Electronic structure and bonding of the blue copper site in plastocyanin. J. Am. Chem. Soc. 107, 4519 – 4529.
117 Pierloot, K., De Kerpel, J. O. A., Ryde, U. and Roos, B. O. (1997) Theoretical study of the electronic spectrum of plastocyanin. J. Am. Chem. Soc. 119, 218 – 226.
118 Pierloot, K., De Kerpel, J. O. A., Ryde, U., Olsson, M. H. M. and Roos, B. O. (1998) Relation between the structure and spectroscopic properties of blue copper proteins. J. Am. Chem. Soc. 120, 13156 – 13166.
119 van Gastel, M., Coremans, J. W. A., Sommerdijk, H., van Hemert, M. C. and Groenen, E. J. J. (2002) An *ab initio* quantum-chemical study of the blue-copper site of azurin. J. Am. Chem. Soc. 124, 2035 – 2041.
120 Guss, J. M., Bartunik, H. D. and Freeman, H. C. (1992) Accuracy and precision in protein structure analysis: restrained least squares refinement of the structure of poplar plastocyanin at 1.33 Å resolution. Acta Cryst. B 48, 790 – 811.
121 Cheung, K.-C., Strange, R. W. and Hasnain, S. S. (2000) 3D EXAFS refinement of the Cu site of azurin sheds light on the nature of structural change at the metal centre in an oxidation–reduction process: an integrated approach combining EXAFS and crystallography. Acta. Cryst. D 56, 697 – 704.
122 Hansen, D. F. and Led, J. J. (2006) Determination of the geometric structure of the metal site in a blue copper protein by paramagnetic NMR. Proc. Natl. Acad. Sci. USA 103, 1738 – 1743.
123 Hansen, D. F. and Led, J. J. (2001) Measuring the longitudinal NMR relaxation rates of fast relaxing nuclei using a signal eliminating relaxation filter. J. Magn. Reson. 151, 339 – 346.
124 Bertini, I., Fernández, C. O., Karlsson, B. G., Leckner, J., Luchinat, C., Malmström, B. G., Nersissian, A. M., Pierattelli, R., Shipp, E., Valentine, J. S. and Vila, A. J. (2000) Structural information through NMR hyperfine shifts in blue copper proteins. J. Am. Chem. Soc. 122, 3701 – 3707.
125 Kalverda, A. P., Salgado, J., Dennison, C. and Canters, G. W. (1996) Analysis of the paramagnetic copper(II) site of amicyanin by ^{1}H NMR spectroscopy. Biochemistry 35, 3085 – 3092.
126 Donaire, A., Jiménez, B., Fernández, C. O., Pierattelli, R., Niizeki, T., Moratal, J.-M., Hall, J. F., Kohzuma, T., Hasnain, S. S. and Vila, A. J. (2002) Metal-ligand interplay in blue copper proteins studied by ^{1}H NMR spectroscopy: Cu(II)-pseudoazurin and Cu(II)-rusticyanin. J. Am. Chem. Soc. 124, 13698 – 13708.
127 Vila, A. J. (1994) A ^{1}H NMR NOE study on Co(II) stellacyanin: some clues about the structure of the metal site. FEBS Lett. 355, 15 – 18.
128 Dennison, C. and Sato, K. (2004) Paramagnetic ^{1}H NMR spectrum of the cobalt(II) derivative of spinach plastocyanin. Inorg. Chem. 43, 1502 – 1510.
129 Salgado, J., Jiménez, H. R., Moratal, J. M., Kroes, S., Warmerdam, G. C. M. and Canters, G. W. (1996) Paramagnetic cobalt and nickel derivatives of *Alcaligenes denitrificans* azurin and its M121Q mutant: a ^{1}H NMR study. Biochemistry 35, 1810 – 1819.
130 Salgado, J., Kalverda, A. P., Diederix, R. E. M., Canters, G. W., Moratal, J. M., Lawler, A. T. and Dennison, C. (1999) Paramagnetic NMR investigations of Co(II) and Ni(II) amicyanin. J. Biol. Inorg. Chem. 4, 457 – 467.
131 Fernández, C. O., Niizeki, T., Kohzuma, T. and Vila, A. J. (2003) Metal-ligand interactions in perturbed blue copper sites: a paramagnetic ^{1}H NMR study of Co(II)-pseudoazurin. J. Biol. Inorg. Chem. 8, 75 – 82.
132 Dennison, C. and Harrison, M. D. (2004) The active-site structure of umecyanin, the stellacyanin from horseradish roots. J. Am. Chem. Soc. 126, 2481 – 2489.
133 Taylor, J. P., Hardy, J. and Fischbeck, K. H. (2002) Toxic proteins in neurodegenerative disease. Science 296, 1991 – 1995.
134 Lee, J. C., Langen, R., Hummel, P. A., Gray, H. B. and Winkler, J. R. (2004) α-Synuclein structures from fluorescence energy-transfer kinetics: implications for the role of the protein in parkinson's disease. Proc. Natl. Acad. Sci. USA 101, 16466 – 16471.
135 Bernado, P., Bertoncini, C. W., Griesinger, C., Zweckstetter, M. and Blackledge, M. (2005) Defining long-range order and local disorder in native alpha-synuclein using residual dipolar couplings. J. Am. Chem. Soc. 127, 17968 – 17969.
136 Lee, J. C., Gray, H. B. and Winkler, J. R. (2005) Tertiary contact formation in α-synuclein probed by electron transfer. J. Am. Chem. Soc. 127, 16388 – 16389.
137 Paik, S. R., Shin, H.-J., Lee, J.-H., Chang, C.-S. and Kim, J. (1999) Copper(II)-induced self-oligomerization of α-synuclein. Biochem. J. 340, 821 – 828.
138 Uversky, V. N., Li, J. and Fink, A. L. (2001) Metal-triggered structural transformations, aggregation, and fibrillation of human α-synuclein, J. Biol. Chem. 276, 44284 – 44296.
139 Binolfi, A., Rasia, R. M., Bertoncini, C. W., Ceolin, M., Zweckstetter, M., Griesinger, C., Jovin, T. M. and Fernandez, C. O. (2006) Interaction of α-synuclein with divalent metal ions reveals key differences: a link between structure, binding specificity and fibrillation enhancement. J. Am. Chem. Soc. 128, 9893 – 9901.
140 Rasia, R. M., Bertoncini, C. W., Marsh, D., Hoyer, W., Cherny, D., Zweckstetter, M., Griesinger, C., Jovin, T. M. and Fernandez, C. O. (2005) Structural characterization of copper(II) binding to α-synuclein: insights into the bioinorganic chemistry of parkinson's disease. Proc. Natl. Acad. Sci. USA 102, 4294 – 4299.
141 Sung, Y., Rospigliosi, C. and Eliezer, D. (2006) NMR mapping of copper binding sites in alpha-synuclein. Biochim. Biophys. Acta 1764, 5 – 12.
142 Giasson, B. I., Murray, I. V. J., Trojanowski, J. Q. and Lee, V. M.-Y. (2001) A hydrophobic stretch of 12 amino acid residues in the middle of α-synuclein is essential for filament assembly. J. Biol. Chem. 276, 2380 – 2386.
143 Bertoncini, C. W., Jung, Y.-S., Fernandez, C. O., Hoyer, W., Griesinger, C., Jovin, T. M. and Zweckstetter, M. (2005) Release of long-range tertiary interactions potentiates aggregation of natively unstructured α-synuclein. Proc. Natl. Acad. Sci. USA 102, 1430 – 1435.
144 Prusiner, S. B. (1991) Molecular biology of prion diseases. Science 252, 1515 – 1522.
145 Caughey, B. W., Dong, A., Bhat, K. S., Ernst, D., Hayes, S. F. and Caughey, W. S. (1991) Secondary structure analysis of the scrapie-associated protein PrP 27 – 30 in water by infrared spectroscopy. Biochemistry 30, 7672 – 7680.
146 Pan, K.-M., Baldwin, M., Nguyen, J., Gasset, M., Serban, A., Groth, D., Mehlhorn, I., Huang, Z., Fletterick, R. J., Cohen, F.

E. and Prusiner, S. B. (1993) Conversion of α-helices into β-sheets features in the formation of the scrapie prion proteins. Proc. Natl. Acad. Sci. USA 90, 10962 – 10966.
147 Brown, D. R., Wong, B.-S., Hafiz, F., Clive, C., Haswell, S. J. and Jones, I. M. (1999) Normal prion protein has an activity like that of superoxide dismutase. Biochem. J. 344, 1 – 5.
148 Brown, D. R., Clive, C. and Haswell, S. J. (2001) Antioxidant activity related to copper binding of native prion protein. J. Neurochem. 76, 69 – 76.
149 Wong, B. S., Pan, T., Liu, T., Li, R., Petersen, R. B., Jones, I. M., Gambetti, P., Brown, D. R. and Sy, M. S. (2000) Breakthroughs and views – prion disease: a loss of antioxidant function? Biochem. Biophys. Res. Commun. 275, 249 – 252.
150 Shiraishi, N., Ohta, Y. and Nishikimi, M. (2000) The octapeptide repeat region of prion protein binds Cu(II) in the redox-inactive state. Biochem. Biophys. Res. Commun. 267, 398 – 402.
151 Whittal, R. M., Ball, H. L., Cohen, F. E., Burlingame, A. L., Prusiner, S. B. and Baldwin, M. A. (2000) Copper binding to octarepeat peptides of the prion protein monitored by mass spectrometry. Protein Sci. 9, 332 – 343.
152 Lehmann, S. (2002) Metal ions and prion diseases. Curr. Opin. Chem. Biol. 6, 187 – 192.
153 Brown, D. R. (2001) Prion and prejudice normal protein and the synapse. TRENDS in Neurosci. 24, 85 – 90.
154 Riek, R., Hornemann, S., Wider, G., Billeter, M., Glockshuber, R. and Wüthrich, K. (1996) NMR structure of the mouse prion protein domain PrP (121 – 231). Nature 382, 180 – 182.
155 James, T. L., Liu, H., Ulyanov, N. B., Farr-Jones, S., Zhang, H., Donne, D. G., Kaneko, K., Groth, D., Mehlhorn, I., Prusiner, S. B. and Cohen, F. E. (1997) Solution structure of a 142-residue recombinant prion protein corresponding to the infectious fragment of the scrapie isoform. Proc. Natl. Acad. Sci. USA 94, 10086 – 10091.
156 Donne, D. G., Viles, J. H., Groth, D., Mehlhorn, I., James, T. L., Cohen, F. E., Prusiner, S. B., Wright, P. E. and Dyson, H. J. (1997) Structure of the recombinant full-length hamster prion protein PrP(29-231): the N terminus is highly flexible. Proc. Natl. Acad. Sci. USA 94, 13452 – 13457.
157 Riek, R., Hornemann, S., Wider, G., Glockshuber, R. and Wüthrich, K. (1997) NMR characterization of the full-length recombinant murine prion protein, mPrP(23-231), FEBS Lett 413, 282 – 288.
158 Viles, J. H., Cohen, F. E., Prusiner, S. B., Goodin, D. B., Wright, P. E. and Dyson, H. J. (1999) Copper binding to the prion protein: structural implications of four identical cooperative binding sites. Proc. Natl. Acad. Sci. USA 96, 2042 – 2047.
159 Garnett, A. P. and Viles, J. H. (2003) Copper binding to the octarepeats of the prion protein. J. Biol. Chem. 278, 6795 – 6802.
160 Thompsett, A. R., Abdelraheim, S. R., Daniels, M. and Brown, D. R. (2005) High affinity binding between copper and full-length prion protein identified by two different techniques. J. Biol. Chem. 280, 42750 – 42758.
161 Hornshaw, M. P., McDermott, J. R., Candy, J. M. and Lakey, J. H. (1995) Copper binding to the N-terminal tandem repeat regions of mammalian and avian prion protein. Biochem. Biophys. Res. Commun. 207, 621 – 629.
162 Hornshaw, M. P., McDermott, J. R., Candy, J. M. and Lakey, J. H. (1995) Copper binding to the N-terminal tandem repeat region of mammalian and avian prion protein: structural studies using synthetic peptides. Biochem. Biophys. Res. Commun. 214, 993 – 999.
163 Brown, D. R., Qin, K., Herms, J. W., Madlung, A., Manson, J., Strome, R., Fraser, P. E., Kruck, T., Bohlen, A., Schulz-Schaeffer, W., Giese, A., Westaway, D. and Kretzschmar, H. (1997) The cellular prion protein binds copper *in vivo*. Nature 390, 684 – 687.
164 Stöckel, J., Safar, J., Wallace, A. C., Cohen, F. E. and Prusiner, S. B. (1998) Prion protein selectively binds copper(II) ions. Biochemistry 37, 7185 – 7193.
165 Aronoff-Spencer, E., Burns, C. S., Avdievich, N. I., Gerfen, G. J., Peisach, J., Antholine, W. E., Ball, H. L., Cohen, F. E., Prusiner, S. B. and Millhauser, G. L. (2000) Identification of the Cu^{2+} binding sites in the N-terminal domain of the prion protein by EPR and CD spectroscopy. Biochemistry 39, 13760 – 13771.
166 Jackson, G. S., Murray, I., Hosszu, L. L. P., Gibbs, N., Waltho, J. P., Clarke, A. R. and Collinge, J. (2001) Location and properties of metal-binding sites on the human prion protein. Proc. Natl. Acad. Sci. USA 98, 8531 – 8535.
167 Gaggelli, E., Bernardi, F., Molteni, E., Pogni, R., Valensin, D., Valensin, G., Remelli, M., Luczkowski, M. and Kozlowski, H. (2005) Interaction of the human prion PrP(106-126) sequence with copper(II), manganese(II), and zinc(II): NMR and EPR studies. J. Am. Chem. Soc. 127, 996 – 1006.
168 Bocharova, O. V., Breydo, L., Salnikov, V. V. and Baskakov, I. V. (2005) Copper(II) inhibits in vitro conversion of prion protein into amyloid fibrils. Biochemistry 44, 6776 – 6787.
169 Weissmann, C. (2004) The state of the prion. Nat. Rev. Microbiol. 2, 861 – 871.
170 Baskakov, I. V. and Bocharova, O. V. (2005) In vitro conversion of mammalian prion protein into amyloid fibrils displays unusual features. Biochemistry 44, 2339 – 2348.
171 Pan, K.-M., Stahl, N. and Prusiner, S. B. (1992) Purification and properties of the cellular prion protein from syrian hamster brain. Protein Sci. 1, 1343 – 1352.
172 Wadsworth, J. D. F., Hill, A. F., Joiner, S., Jackson, G. S., Clarke, A. R. and Collinge, J. (1999) Strain-specific prion-protein conformation determined by metal ions. Nat. Cell Biol. 1, 55 – 59.
173 Brown, D. R., Hafiz, F., Glasssmith, L. L., Wong, B.-S., Jones, I. M., Clive, C. and Haswell, S. J. (2000) Consequences of manganese replacement of copper for prion protein function and proteinase resistance. EMBO J. 19, 1180 – 1186.
174 Jones, C. E., Klewpatinond, M., Abdelraheim, S. R., Brown, D. R. and Viles, J. H. (2005) Probing Cu^{2+} binding to the prion protein using diamagnetic $nickel^{2+}$ and ^1H NMR: the unstructured N-terminus facilitates the coordination of six $copper^{2+}$ ions at physiological concentrations. J. Mol. Biol. 346, 1393 – 1407.
175 Treiber, C., Simons, A. and Multhaup, G. (2006) Effect of copper and manganese on the de novo generation of protease-resistant prion protein in yeast cells. Biochemistry 45, 6674 – 6680.
176 Tsenkova, R. N., Iordanova, I. K., Toyoda, K. and Brown, D. R. (2004) Prion protein fate governed by metal binding. Biochem. Biophys. Res. Commun. 325, 1005 – 1012.
177 Nomura, M., Kobayashi, T., Kohno, T., Fujiwara, K., Tenno, T., Shirakawa, M., Ishizaki, I., Yamamoto, K., Matsuyama, T., Mishima, M. and Kojima, C. (2004) Paramagnetic NMR study of Cu^{2+}-IDA complex localization on protein surface and its application to elucidate long distance information. FEBS Lett. 566, 157 – 161.
178 Jensen, M. R. and Led, J. J. (2006) Metal-protein interactions: structure information from Ni^{2+}-induced pseudocontact shifts in a native nonmetalloprotein. Biochemistry 45, 8782 – 8787.
179 Holmgren, A. (1985) Thioredoxin. Annu. Rev. Biochem. 54, 237 – 271.
180 180 van Holde, M. (1990) Biochemistry, p. 140. Benjamin/Cummings, Mento Park.
181 DeLano, W. L. (2002) The PyMOL Molecular Graphics System. DeLano Scientific, San Carlos.
182 Koradi, R., Billeter, M. and Wüthrich, K. (1996) MOLMOL: A program for display and analysis of macromolecular structures. J. Mol. Graphics 14, 51 – 55.